AAS 18-308

CLOSED-FORM OPTIMAL IMPULSIVE CONTROL OF SPACECRAFT FORMATIONS USING REACHABLE SET THEORY

Michelle Chernick*, Simone D'Amico†

This paper addresses the spacecraft relative orbit reconfiguration problem of minimizing the delta-v cost of a set of impulsive control actions while achieving a desired state in fixed time. The problem is cast into relative orbit element space, which yields insight into the geometry of relative motion and allows for the straightforward inclusion of perturbations in linear time-variant form. Reachable set theory is used to translate the cost-minimization problem into a geometric path-planning problem and to formulate a novel metric, the reachable delta-v minimum, for assessing the optimality of a proposed maneuver scheme. This metric informs the derivation of closed-form globally energy-optimal maneuver schemes in eccentric and near-circular orbits. The proposed algorithms are tested and validated in high-fidelity simulations. For the first time in literature, general, closed-form, globally optimal maneuver schemes for relative orbit reconfiguration are derived in eccentric orbits. Furthermore, the newly proposed method based on reachable set theory can be applied to any linear time-variant dynamics system.

INTRODUCTION

Distributed space systems enable advanced missions in fields such as astronomy and astrophysics, planetary science, and space infrastructure by employing the collective usage of two or more cooperative spacecraft. Proposed formation flying missions in eccentric orbits introduce new challenges for spaceborne control architectures, such as efficiency (reduced on-board processing power and propellant), autonomy (no ground-in-the-loop), and operational constraints (interference with payload, predictability).[1] To address these challenges, this work develops globally-optimal closed-form solutions to the problem of minimizing the delta-v cost of a set of impulsive control actions while accomplishing a fixed desired satellite relative orbit configuration in fixed time.

In literature, most approaches to finding impulsive maneuver schemes that accomplish the fixed-time, fixed-end condition reconfiguration fall into three categories: direct optimization techniques, in-direct optimization techniques, and closed-form solutions. For spaceborne applications, closed-form solutions are favored because they are simple, predictable, and computationally efficient. Numerous authors have developed closed-form solutions in Hill's coordinates, but their solutions are limited to only near-circular orbits.[2,3] In fact, this limitation is innate in the equations of relative motion in Hill's coordinates, called the Hill-Clohessy-Wiltshire equations (HCW). They are accurate only in near-circular orbits and for small separations between the spacecraft. However, these limitations are easily overcome by using a different state representation, called relative orbit elements (ROE). As will be discussed in the following section, use of the ROE state representation allows for the derivation of simple, high-fidelity solutions to the spacecraft formation control problem. The ROE state inherently enables the linearization of the equations of relative motion with minimal loss of accuracy,[4] and it is this linearization that allows for application of reachable set theory to enable a geometric solution of the resulting optimal control problem. Despite the benefits of using the ROE state representation, few authors have solved the reconfiguration problem in closed-form using ROE. Gaias and D'Amico[5,6] proposed a set of closed-form guidance and control algorithms for optimal control in near-circular orbits. Chernick and D'Amico[7] extended these algorithms to include perturbations due to Earth's oblateness (J_2) in near-circular orbits and developed control solutions in eccentric unperturbed orbits. Vaddi et al.[8] proposed analytical solutions to the optimal reconfiguration problem,

*Ph.D. Candidate, Space Rendezvous Laboratory, Aeronautics and Astronautics, 496 Lomita Mall
†Assistant Professor, Space Rendezvous Laboratory, Aeronautics and Astronautics, 496 Lomita Mall

but only for control of the in-plane orbital elements in near-circular orbits. Schaub and Alfriend[9] developed an impulsive feedback controller to establish mean orbit element differences. These solutions (and their optimality) are case-specific and have not yet been advanced to include other perturbations. Direct optimization techniques allow for a greater degree of generality because the optimal control problem can be formulated with the times, magnitudes, and directions as variables.[10] Though widely applicable, direct optimization techniques are not guaranteed to converge to a global optimum because the minimum cost is generally a non-convex function of the control action times.[11] In addition, direct optimization techniques do not provide insight into the maneuver optimality and so do not necessarily represent the best solution for satellite on-board implementation. Therefore, the majority of numerical approaches in literature utilize indirect optimization techniques, taking advantage of the characteristics of the so-called primer and dual pair of the optimal control problem. For example, Roscoe et al.[12] designed an optimal algorithm for eccentric perturbed orbits based on Lawden's primer vector theory and Pontryagin's optimal control.[13] This algorithm involves an iterative process that depends on a good initial guess and yields large computational loads. Gilbert and Harasty[14] proposed a different approach to indirect optimization based on reachable set theory, which converges to a globally optimal sequence of impulsive control inputs for problems with norm-like constant cost functionals. Koenig[15] generalized Gilbert's algorithm to time-variant cost functions with the only restriction that the cost function be represented as the integral of a time-variant norm-like function of the control input vector. In optimal control and robotics applications, reachable set theory is commonly used to assess cost-reachability and safety.[16] However, the theory is only implemented as a numerical assessment tool. Instead, this paper shows that reachable set theory can be used not just to assess the cost of a maneuver scheme, but as a geometric tool to derive the closed-form maneuver scheme itself.

Here, closed-form solutions to the satellite relative orbit reconfiguration problem are derived leveraging domain specific knowledge and reachable set theory. This work improves upon the shortcomings of the current literature through three main contributions to the state-of-the-art. First, a new metric called the reachable delta-v minimum, δv_{min}, is derived using the linear scaling properties of the reachable sets in order to better assess maneuver scheme optimality. Second, closed-form maneuver schemes in eccentric unperturbed orbits and near-circular perturbed orbits are derived. Third, the maneuver schemes are validated by comparison to Koenig's numerical optimization algorithm[15] and by numerical integration of the Gauss Variational Equations. What follows is the formal statement of the energy-optimal formation control problem.

PROBLEM STATEMENT

Without loss of generality, a formation here consists of two satellites: the chief, which defines the reference orbit and is uncontrolled, and the deputy, which is controlled by a 3D thrust input. The relative motion between two satellites in a formation is commonly defined in terms of relative position and velocity in the Hill's coordinate frame (also called radial/along-track/cross-track coordinates, or RTN), whose origin is found at the chief's center of mass. The RTN frame is defined by the basis $[o_r, o_t, o_n]$, where o_r is aligned with the radial direction and positive outward, o_n is aligned with the chief angular momentum vector and positive in the orbit normal direction, and o_t completes the right-handed triad. However, the relative motion can be equivalently described using combinations of non-dimensional orbit elements of the chief and deputy, called relative orbit elements (ROE), $\delta\boldsymbol{\alpha} = \delta\boldsymbol{\alpha}(\boldsymbol{\alpha}_c, \boldsymbol{\alpha}_d)$. The benefits of using the ROE state representation are numerous. First, the homogeneous, unperturbed solution to the ROE dynamics equations is the trivial solution of the Keplerian two-body problem, $\delta\boldsymbol{\alpha} = \text{const.}$, whereas there is no available unperturbed solution to the equations of relative motion in Hill's coordinates.[7] In addition, in the presence of perturbations, a state based on ROE slowly varies in time, whereas Hill's coordinates vary rapidly. Secular and long-period effects of perturbing forces are simply included in the equations of relative motion for the ROE state by use of a state transition matrix (STM), $\boldsymbol{\Phi}(t_j, t_i)$. The STM propagates the state forward in time, while the control input matrix, $\boldsymbol{\Gamma}(t_k)$, represents the effect of a 3D control input $\delta\boldsymbol{v}_k$ at time t_k. With this notation in mind, the linearized dynamics that govern the reconfiguration from an initial set of ROE, $\delta\boldsymbol{\alpha}_0$, to a final desired set of ROE, $\delta\boldsymbol{\alpha}_f$, under the influence of p impulsive maneuvers can be written as

$$\delta\boldsymbol{\alpha}_f = \boldsymbol{\Phi}(t_f, t_0)\delta\boldsymbol{\alpha}_0 + \sum_{k=1}^{p} \boldsymbol{\Phi}(t_f, t_k)\boldsymbol{\Gamma}(t_k)\delta\boldsymbol{v}_k. \tag{1}$$

Given an initial set of chief orbital elements, $\boldsymbol{\alpha}_{c,0}$, and an initial set of ROE, $\delta\boldsymbol{\alpha}_0$, the fixed-time, fixed-end conditions relative orbit reconfiguration problem is defined by a desired final set of ROE, $\delta\boldsymbol{\alpha}_f \in \mathbb{R}^6$, and a

reconfiguration time span T. With these reconfiguration parameters, the optimal control problem to be solved in this paper is

$$\text{Minimize } \sum_{k=1}^{p} ||\delta \boldsymbol{v}_k||_2 \qquad \text{subject to } \Delta\delta\bar{\boldsymbol{\alpha}} = \sum_{k=1}^{p} \boldsymbol{\Phi}(t_f, t_k)\boldsymbol{\Gamma}(t_k)\delta\boldsymbol{v}_k,\, t_k \in T \tag{2}$$

where a pseudo-state $\Delta\delta\bar{\boldsymbol{\alpha}}$ is introduced as $\Delta\delta\bar{\boldsymbol{\alpha}} = \delta\boldsymbol{\alpha}_f - \boldsymbol{\Phi}(t_f, t_0)\delta\boldsymbol{\alpha}_0$ to simplify notation. The next section outlines the dynamics of relative motion as they apply to the adopted ROE state definition.

BACKGROUND

Astrodynamics of Relative Motion

In this paper, the state representation of choice is the 6D quasi-nonsingular ROE, given[7,17] as

$$\delta\boldsymbol{\alpha} = \begin{bmatrix} \delta a \\ \delta\lambda_e \\ \delta e_x \\ \delta e_y \\ \delta i_x \\ \delta i_y \end{bmatrix} = \begin{bmatrix} \delta a \\ \delta\lambda_e \\ \delta e\cos\varphi \\ \delta e\sin\varphi \\ \delta i\cos\theta \\ \delta i\sin\theta \end{bmatrix} = \begin{bmatrix} \frac{a_d - a_c}{a_c} \\ M_d - M_C + \eta(\omega_d - \omega_c + (\Omega_d - \Omega_c)\cos i_c) \\ e_d\cos\omega_d - e_c\cos\omega_c \\ e_d\sin\omega_d - e_c\sin\omega_c \\ i_d - i_c \\ (\Omega_d - \Omega_c)\sin i_c \end{bmatrix}. \tag{3}$$

It is termed quasi-nonsingular because the state is valid for circular chief orbits ($e_c = 0$) but becomes singular for strictly equatorial chief orbits ($i_c = 0$). Apart from the modified relative mean longitude $\delta\lambda_e$, it is the same state used for Guidance, Navigation, and Control (GNC) and orbit design on multiple formation flying missions such as PRISMA[18] and TanDEM-X.[19] In order to derive closed-form maneuver schemes in the ROE state representation, it is necessary to first find the STM and control input matrix that propagate the dynamics. Koenig et al.'s approach[20] is used to derive the STM from t_0 to t_f for the quasi-nonsingular ROE (provided in Appendix A, Eq. (32)). The change in the mean ROE due to an impulsive maneuver $\delta\boldsymbol{v}_k$ is described by the control input matrix $\boldsymbol{\Gamma}(t_k)$ and derived from the Gauss Variational Equations (GVE). The GVE describe the rate of change of the osculating orbital elements $\boldsymbol{\alpha}_{osc}$ as a function of perturbing accelerations in the RTN frame. The effect of an impulsive maneuver $\delta\boldsymbol{v}_k$ on the osculating ROE is found by integrating the GVE over the duration of the maneuver with the assumption that the orbital elements are constant, and can be written in matrix form using the chain rule as $\Delta\delta\boldsymbol{\alpha}_{osc} = \frac{\partial\delta\boldsymbol{\alpha}(\boldsymbol{\alpha}_{c,osc},\boldsymbol{\alpha}_{d,osc})}{\partial\boldsymbol{\alpha}_{d,osc}} \frac{\partial\boldsymbol{\alpha}_{d,osc}}{\partial\boldsymbol{v}_{RTN}}\delta\boldsymbol{v}_k$. To employ the same approach for the mean ROE state representation used in this paper, Brouwer's transformation from osculating to mean orbital elements f_{mean} is applied.[21] The partial derivatives of f_{mean} with respect to the osculating orbital elements form a Jacobian matrix which is near identity. For the mean ROE state, the control input matrix is then

$$\boldsymbol{\Gamma}(\boldsymbol{\alpha}_c) \approx \left.\frac{\partial\delta\boldsymbol{\alpha}(\boldsymbol{\alpha}_c, \boldsymbol{\alpha}_d)}{\partial\boldsymbol{\alpha}_d}\right|_{\boldsymbol{\alpha}_c = \boldsymbol{\alpha}_d} \frac{\partial f_{mean}(\boldsymbol{\alpha}_{d,osc})}{\partial\boldsymbol{\alpha}_{d,osc}} \frac{\partial\boldsymbol{\alpha}_d}{\partial\boldsymbol{v}_{RTN}}, \tag{4}$$

and the effect of an impulsive maneuver on the mean ROE is given by[8] $\Delta\delta\boldsymbol{\alpha} = \boldsymbol{\Gamma}(\boldsymbol{\alpha}_c)\delta\boldsymbol{v}$. The explicit expressions for $\boldsymbol{\Gamma}$ as tailored to the cases of perturbed near-circular and unperturbed eccentric orbits are given in Appendix A in Eqs. (36) and (38). By virtue of the form of $\boldsymbol{\Gamma}$, in the near-circular case, the ROE state is effectively decoupled; in-plane maneuvers (radial, tangential) affect only the in-plane ROE, δa, $\delta\lambda$, and $\delta\boldsymbol{e}$, and out-of-plane maneuvers (normal) affect only the out-of-plane ROE, $\delta\boldsymbol{i}$. In contrast, in the eccentric case, the relative eccentricity vector is affected by maneuvers in the normal direction, so an inherent decoupling cannot be claimed for the ROE state as defined in Eq. (3). However, this work assumes that if a correction in the relative inclination vector is required, an out-of-plane maneuver is performed independently from the in-plane maneuvers. The effect of that maneuver on the relative eccentricity vector is subtracted from the desired change in the relative eccentricity vector if performed before the in-plane maneuvers or vice versa. Note that the decoupling of the ROE state does not imply a decoupling of the optimal control problem; because the cost function is two-norm, the control problem is fully coupled in general.

Reachable Set Theory

This section provides an introduction to reachable set theory, which will be used to derive a simple geometric optimality criteria and closed-form optimal reconfiguration schemes. Let $U(c)$ be the set of all control actions in

RTN whose magnitude is less than or equal to c. $S(c,t_j)$ is the set of pseudo-states $\Delta\delta\bar{\boldsymbol{\alpha}}$ that can be reached at the end of the reconfiguration T given a single control action $\boldsymbol{u}$ of magnitude less than or equal to c at time t_j,

$$S(c,t_j) = \{\Delta\delta\bar{\boldsymbol{\alpha}} : \Delta\delta\bar{\boldsymbol{\alpha}} = \boldsymbol{\Phi}(t_f,t_j)\boldsymbol{\Gamma}(t_j)\boldsymbol{u}, \boldsymbol{u} \in U(c)\}, t_j \in T. \tag{5}$$

$S(c,T)$ is the set of pseudo-states $\Delta\delta\bar{\boldsymbol{\alpha}}$ that can be reached at the end of the reconfiguration time T given a single control action of magnitude less than or equal to c at any time in T, given by

$$S(c,T) = \bigcup_{t_j \in T} S(c,t_j). \tag{6}$$

Finally, $S^*(c,T)$ is the set of pseudo-states $\Delta\delta\bar{\boldsymbol{\alpha}}$ that can be reached at the end of the reconfiguration T given $p \geq 1$ control actions of total magnitude less than or equal to c at any time in T. For any $\Delta\delta\bar{\boldsymbol{\alpha}}^* \in S^*(c,T)$, there must exist a set of p control actions $\{\boldsymbol{u}_1, ..., \boldsymbol{u}_p\}$ executed at times $\{t_1, ..., t_p\}$ respectively that satisfies $\Delta\delta\bar{\boldsymbol{\alpha}}^* = \sum_{k=1}^{p} \boldsymbol{\Phi}(t_f,t_k)\boldsymbol{\Gamma}(t_k)\boldsymbol{u}_k$, $\sum_{k=1}^{p} ||\boldsymbol{u}_k||_2 \leq c, t_k \in T$. Because the cost of a control action scales linearly with its magnitude and $\boldsymbol{\Phi}(t_f,t_k)\boldsymbol{\Gamma}(t_k)\boldsymbol{u}_k$ is an element of $S(c,T)\ \forall t_k$, $S^*(c,T)$ can be defined as

$$S^*(c,T) = \{\Delta\delta\bar{\boldsymbol{\alpha}}^* : \Delta\delta\bar{\boldsymbol{\alpha}}^* = \sum_{k=1}^{p} c_k \Delta\delta\bar{\boldsymbol{\alpha}}_k, \Delta\delta\bar{\boldsymbol{\alpha}}_k \in S(c,T), c_i \geq 0, \sum_{k=1}^{p} c_k = 1\}, \tag{7}$$

which is the definition of the convex hull of $S(c,T)$. Based on this definition, a pseudo-state that lies on the boundary of the convex hull $S^*(c,T)$ is reachable with total delta-v equal to c. There are three important properties of the reachable set that will be leveraged to derive reachable delta-v minima and energy-optimal maneuver schemes. First, the reachable set is a linear function of a control action for linear time-variant (LTV) systems, so the reachable set scales linearly with cost. This allows for the development of a very simple optimality condition; if δv_{min} is the optimal cost for a given reconfiguration, then $\Delta\delta\bar{\boldsymbol{\alpha}}$ will lie on the boundary of $S^*(\delta v_{min}, T)$. Second, it is clear from the definitions above that if and only if a desired endpoint is on the boundary of both S and S^* for a given reconfiguration, the reconfiguration can be achieved with a single maneuver. This fact proves useful in categorizing and deriving closed-form maneuver schemes because it defines the minimum number of maneuvers required. Third, a 2n-dimensional state can be projected into n 2D planes and analyzed separately without loss of generality. A proof of this claim follows by use of an $n = 2$ example consistent with the in-plane ROE state. In fact, it will be shown that the total cost of the entire reconfiguration is driven by one of these 2D planes.

Suppose that a desired reconfiguration given by $[\Delta\delta\bar{x}_{1,des}, \Delta\delta\bar{x}_{2,des}, \Delta\delta\bar{y}_{1,des}, \Delta\delta\bar{y}_{2,des}]$ is split into the 2D $\Delta\delta\bar{\boldsymbol{x}}_{des}$ reconfiguration and the 2D $\Delta\delta\bar{\boldsymbol{y}}_{des}$ reconfiguration, and that the minimum delta-v required to achieve each 2D reconfiguration independently is known. Let the minimum delta-v required to achieve a desired change in $\delta\boldsymbol{x}$ be called $\delta v_{min,\delta\boldsymbol{x}}$, and let the minimum delta-v required to achieve a desired change in $\delta\boldsymbol{y}$ be called $\delta v_{min,\delta\boldsymbol{y}}$. The minimum delta-v required to achieve the entire desired reconfiguration is

$$\delta v_{min} \geq \max\{\delta v_{min,\delta\boldsymbol{x}}, \delta v_{min,\delta\boldsymbol{y}}\}. \tag{8}$$

Proof. Suppose $\delta v_{min,\delta\boldsymbol{x}} > \delta v_{min,\delta\boldsymbol{y}}$. If $S^*(\delta v_{min,\delta\boldsymbol{x}}, T)$ is computed in both planes using Eq. (7), the desired pseudo-state will lie on its boundary in the $\Delta\delta\boldsymbol{x}$ plane by definition. Because $\delta v_{min,\delta\boldsymbol{x}} > \delta v_{min,\delta\boldsymbol{y}}$, the desired pseudo-state will lie inside the boundary of $S^*(\delta v_{min,\delta\boldsymbol{x}}, T)$ in the $\Delta\delta\boldsymbol{y}$ plane. Therefore, the desired change in $\delta\boldsymbol{x}$ is reachable (see Figure 1a). Now suppose $S^*(\delta v_{min,\delta\boldsymbol{y}}, T)$ is computed in both planes. In the $\Delta\delta\boldsymbol{y}$ plane, the desired pseudo-state now lies on the boundary of the convex hull by definition (see Figure 1b). However, in the $\Delta\delta\boldsymbol{x}$ plane, the desired pseudo-state is outside of the reachable region, because the delta-v required to reach it is larger than the delta-v that defines the boundary of the convex hull. Therefore, the delta-v for the total reconfiguration is no less than than $\delta v_{min,\delta\boldsymbol{x}}$. ∎

The inequality in Eq. (8) stems from the fact that projecting a higher dimensional space onto a lower dimensional space inherently loses information about the shape of that space. For example, it is not possible to know whether a circle was projected from a cone or a cylinder. Nonetheless, it is possible to quantify when the expression in Eq. (8) is an equality. The minimum delta-v of the entire reconfiguration equals $\delta v_{min,\delta\boldsymbol{x}}$ when the desired pseudo-state lies in $S_n^*(\delta v_{min,\delta\boldsymbol{x}}, T_{opt,\delta\boldsymbol{x}})$. S_n^* is computed in using Eq. (7) in both the $\Delta\delta\boldsymbol{x}$ and the $\Delta\delta\boldsymbol{y}$ planes, where $T_{opt,\delta\boldsymbol{x}}$ is the set of optimal maneuver times. The subscript n in S_n^* denotes a nested

reachable set, which is generated using a subset of times in the total reconfiguration time and is therefore itself a subset of the reachable set S^*. If S_n^* includes the desired pseudo-state when mapped onto the other 2D plane(s), the expression in Eq. (8) is an equality. A more in depth discussion of how to find those optimal times for the quasi-nonsingular ROE follows in the "Closed-Form Maneuver Schemes" section.

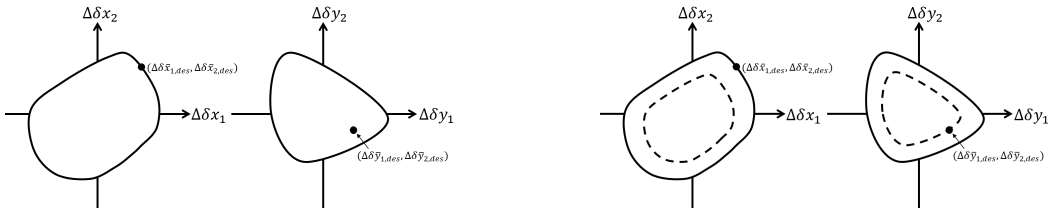

(a) Reachable sets in both planes defined by $\delta v_{min,\delta\boldsymbol{x}}$, represented by the solid line

(b) Reachable sets in both planes defined by $\delta v_{min,\delta\boldsymbol{y}}$, represented by the dashed line

Figure 1: Illustration of proof that total cost of entire reconfiguration is driven by one 2D plane.

The analysis above proves Eq. (8) for a general state representation and LTV system, but this paper focuses on the quasi-nonsingular ROE. In ROE space, the plane whose total required delta-v defines the maximum in Eq. (8) is referred to as the dominant plane, and the individual ROE whose total required delta-v defines the maximum within the plane is known as the dominant ROE. For the ROE state, the $\Delta\delta\boldsymbol{x}$ plane corresponds to the $(\Delta\delta\lambda, \Delta\delta a)$ plane (also called the $\Delta\delta\boldsymbol{a}$ plane), and the $\Delta\delta\boldsymbol{y}$ plane corresponds to the $\Delta\delta\boldsymbol{e}$ plane. Dominance in the $\Delta\delta\boldsymbol{e}$ plane is assessed in terms of the 2-norm of the vector, not as its separate directional components. The third plane is the $\Delta\delta\boldsymbol{i}$ plane, which is decoupled from the other two planes under the assumption in the previous section that an out-of-plane maneuver occurs independently.

Using the results of the proof above, cost optimality is reduced from a 6D problem to three 2D problems that can be analyzed separately. The next section categorizes reconfigurations in each 2D plane using this simplification according to number of maneuvers required. This analysis drives the derivation of the reachable delta-v minima.

Analysis of Reachable Sets in ROE Space

Recall, if a desired pseudo-state $\Delta\delta\bar{\boldsymbol{\alpha}}_{des}$ lies on the boundary of $S(c,T)$ and $S^*(c,T)$ for some cost c, the reconfiguration can be achieved with a single maneuver. If the desired pseudo-state lies only on $S^*(c,T)$'s boundary, then the number of maneuvers required is no more than the size of the state. Looking at the three 2D planes separately, reconfigurations can be categorized based on whether they can be achieved with one or two maneuvers by determining the times $\in T$ where $S(c,t)$ intersects the boundary of $S^*(c,T)$ intersect, where S and S^* are computed with Eqs. (6) and (7), respectively. The near-circular case is found by substituting $\boldsymbol{\Phi}$ (Eq. (34)) and $\boldsymbol{\Gamma}$ (Eq. (36)) into the equations for S and S^* and is shown in Figure 2.

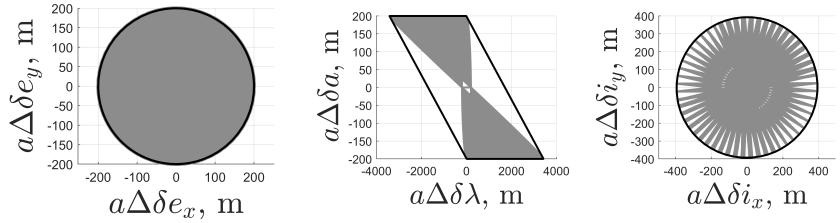

(a) $\Delta\delta\boldsymbol{e}$ plane

(b) $\Delta\delta\boldsymbol{a}$ plane

(c) $\Delta\delta\boldsymbol{i}$ plane

Figure 2: $S(1,T)$ (gray) and convex hull $S^*(1,T)$ (solid line) boundary in near-circular orbits.

In the $\Delta\delta\boldsymbol{e}$ and $\Delta\delta\boldsymbol{i}$ planes (Figure 2a and 2c), the boundary of the gray shaded region S is equal to the boundary of S^*, the solid black line, so all desired pseudo-states can be reached with a single maneuver. In the

$\Delta\delta\boldsymbol{a}$ plane in Figure 2b, any pseudo-state that lies on the top or bottom surface of the reachable set parallelogram can be reached with one maneuver, because S and S^* share the boundary. However, on the left and right sides of the shape, for dominant $\delta\lambda$ reconfigurations, a minimum of two maneuvers is required. Thus, the reachable delta-v minimum in the case of dominant $\delta\lambda$ is a function of two maneuvers.

The eccentric case (Figure 3), as found by substituting $\mathbf{\Phi}$ (Eq. (37)) and $\mathbf{\Gamma}$ (Eq. (38)) into the equations for S and S^*, is more restrictive. In the $\Delta\delta\boldsymbol{e}$ plane (Figure 3a), S and S^* are equal except for a very small region near the axis of symmetry of the reachable set which appears only for very high eccentricities (i.e. $e > 0.85$). As long as the desired pseudo-state does not lie within this region, the point can be reached with a single maneuver. In the $\Delta\delta\boldsymbol{a}$ plane (Figure 3b), unlike in the near-circular case, there are only a few locations on the top/bottom surface of the parallelogram that are reachable with a single maneuver. The $\Delta\delta\boldsymbol{i}$ planes is similar to the $\Delta\delta\boldsymbol{e}$ plane, but with a slightly larger region where S and S^* disconnect.

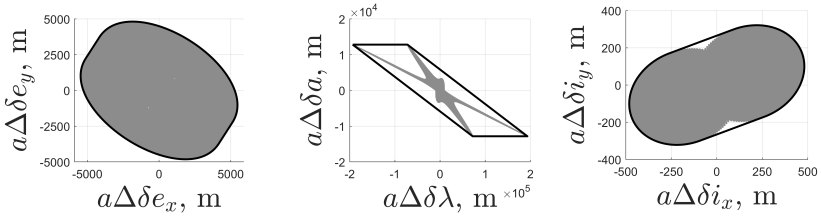

(a) $\Delta\delta\boldsymbol{e}$ plane (b) $\Delta\delta\boldsymbol{a}$ plane (c) $\Delta\delta\boldsymbol{i}$ plane

Figure 3: $S(1,T)$ (gray) and convex hull $S^*(1,T)$ (solid line) boundary in eccentric orbits.

The simple geometry of the reachable sets in ROE space above is the basis for derivation of the reachable delta-v minima and closed-form maneuver schemes in this paper. In fact, comparing reachable sets across state representations provides further justification for using ROE. Figures 4 and 5 show the reachable sets in Hill's coordinates, the most common relative state representation. The reachable sets in the $\delta r, \delta v_r$, $\delta t, \delta v_t$, and $\delta n, \delta v_n$ planes are generated using the HCW STM[22] in near-circular orbits and the Yamanaka-Ankerson (YA) STM[23] in eccentric orbits.

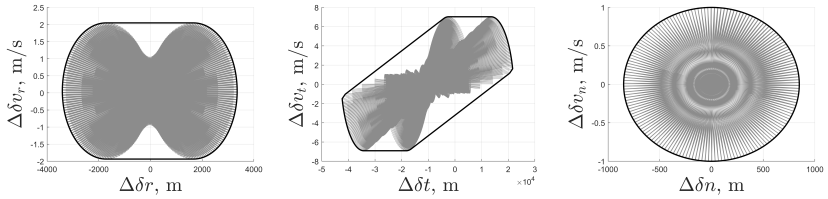

(a) $\delta r, \delta v_r$ plane (b) $\delta t, \delta v_t$ plane (c) $\delta n, \delta v_n$ plane

Figure 4: Reachable set $S(1,T)$ (gray) and convex hull $S^*(1,T)$ boundary (solid black line) in $\delta r, \delta v_r$, $\delta t, \delta v_t$, and $\delta n, \delta v_n$ planes in near-circular orbits, generated using HCW STM.

The most notable difference is between the reachable sets in near-circular orbits. The ROE reachable sets in Figure 2 are symmetric shapes with linear boundaries, which enables the derivation of differentiable parametric equations to describe the boundary of the convex hull. The HCW reachable sets in Figure 4 do not take a similarly simple form. For example, though the reachable set in the $\delta t, \delta v_t$ plane (Figure 4b) is symmetric, the boundary of the convex hull is not a common polygon or circle. Consequently, the range of pseudo-states achievable with a single maneuver is not easily derived directly from a geometric interpretation. Only the $\delta n, \delta v_n$ reachable set (Figure 4c) has a shape that is comparably simple to the ROE reachable sets.

The same is true in the comparison between the ROE reachable sets for nonzero eccentricity in Figure 3 and the YA reachable sets in Figure 5. When the eccentricity of the chief orbit is nonzero, the ROE reachable sets maintain simple geometry, while the YA reachable sets do not. This comparison furthers the claim that using ROE simplifies the relative motion reconfiguration problem.

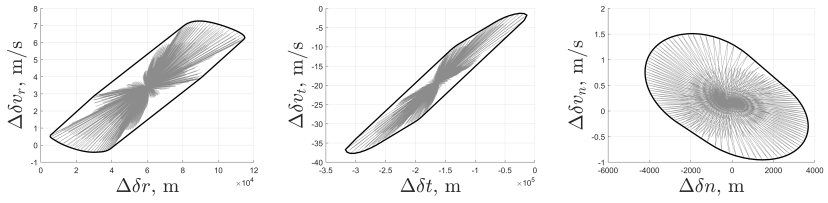

(a) $\delta r, \delta v_r$ plane (b) $\delta t, \delta v_t$ plane (c) $\delta n, \delta v_n$ plane

Figure 5: Reachable set $S(1,T)$ (gray) and convex hull $S^*(1,T)$ boundary (solid black line) in $\delta r, \delta v_r$, $\delta t, \delta v_t$, and $\delta n, \delta v_n$ planes in eccentric orbits, generated using YA STM.

The intuition gained from analyzing the simplicity of the ROE reachable sets will be used to define dominance cases, derive closed-form expressions for the reachable delta-v minima, and develop globally optimal closed-form maneuver schemes in the sections that follow.

REACHABLE DELTA-V MINIMA

This section will derive closed-form expressions and their applicability for the reachable delta-v minima in eccentric and near-circular orbits. First, this section lays out the general methodology used to derive the reachable delta-v minimum. Second, the general methodology is applied to a specific example. Finally, the explicit closed-form expressions of the reachable delta-v minima are provided in tables for all dominance cases in eccentric unperturbed and near-circular J_2 perturbed orbits. In previous work, a metric called the delta-v lower bound, δv_{lb}, was used to quantify optimality.[5,7] As the name suggests, δv_{lb} is a lower bound on the delta-v required for a given reconfiguration. It was derived assuming the use of only tangential maneuvers because of their inherent efficiency, which restricts the definition to reconfigurations that can be accomplished using only tangential maneuvers. It is therefore appropriate to define a new metric, called the reachable minimum delta-v, δv_{min}, which is the minimum delta-v required to achieve a desired reconfiguration. Recall, this expression was used in the proof that an $2n$-dimensional (2nD) state can be decoupled into n 2D planes. Leveraging the fact that the state can be decoupled into three planes, domain specific knowledge, and the linear scaling properties of the reachable set, general closed-form expressions for δv_{min} in each dominance case can be derived. The general methodology follows, given a desired pseudo-state, $\Delta\delta\bar{\boldsymbol{\alpha}}_{des}$ (Eq. (2)) and reconfiguration time, T.

General Methodology

The general methodology to derive closed-form expressions for the reachable delta-v minimum for in-plane reconfigurations is based on four steps as outlined in the following. A parameter with notation $(.)^*$ is a specific instance of the variable $(.)$.

1. Find the expression for the maneuver of magnitude one, $\delta\boldsymbol{v}^*$, that achieves the largest change in ROE. $\delta\boldsymbol{v}^*$ is a function of the true anomaly, ν, in eccentric orbits, or of the mean argument of latitude, u, in near-circular orbits. The tangential component of $\delta\boldsymbol{v}^*$, δv_t^* is found by solving for the critical points of $\Delta\delta(.)_x^2 + \Delta\delta(.)_y^2$, where the subscripts x, y denote the axes of the 2D plane. The radial component, δv_r, is then found by solving the constraint of unitary delta-v, $\delta v_r^2 + \delta v_t^2 = 1$. For out-of-plane reconfigurations, the unitary maneuver magnitude constraint is $\delta v_n^* = 1$. Figure 6a illustrates Step 1, where the solid black line represents $S^*(c,T)$ for an arbitrary c. The effect of the maneuver is represented by the dashed arrow and is a function of the maneuver location along the reference orbit. The desired pseudo-state does not lie on the boundary, so this is not the optimal delta-v, as expected.

2. Solve for the maneuver location, ν^* or u^*, that corresponds to the direction of the desired change. The maneuver location is found by equating the phase of the desired change to the phase of the x,y components of a set of parameterized functions that define the boundary of the convex hull as

$$\tan^{-1}\left(\frac{\Delta\delta(.)_y(\nu, \delta v_t^*(\nu))}{\Delta\delta(.)_x(\nu, \delta v_t^*(\nu))}\right) = \tan^{-1}\left(\frac{\Delta\delta(.)_{y,des}}{\Delta\delta(.)_{x,des}}\right), \tag{9}$$

where the parametric equations are found by propagating the effect of a single maneuver at a given ν (or equivalent time t) using the STM and control input matrix as

$$\begin{bmatrix}\Delta\delta(.)_x(\nu,\delta v_t^*(\nu))\\ \Delta\delta(.)_y(\nu,\delta v_t^*(\nu))\end{bmatrix} = \boldsymbol{\Phi}(t_f,t)\boldsymbol{\Gamma}(t) = \begin{cases}\begin{bmatrix}\Delta\delta\lambda(\nu,\delta v_t^*(\nu))\\ \Delta\delta a(\nu,\delta v_t^*(\nu))\end{bmatrix} & \text{in the } \Delta\delta a, \Delta\delta\lambda \text{ plane, by}\\ \begin{bmatrix}\Delta\delta e_x(\nu,\delta v_t^*(\nu))\\ \Delta\delta e_y(\nu,\delta v_t^*(\nu))\end{bmatrix} & \text{in the } \Delta\delta\boldsymbol{e} \text{ plane, and by}\\ \begin{bmatrix}\Delta\delta i_x(\nu,\delta v_n^*(\nu))\\ \Delta\delta i_y(\nu,\delta v_n^*(\nu))\end{bmatrix} & \text{in the } \Delta\delta\boldsymbol{i} \text{ plane.}\end{cases} \tag{10}$$

Eq. (10) are functions of the maneuver application time t or equivalent angle ν (or in near-circular orbits, u). The explicit form of Eq. (10) is given in the subsections that follow. Step 2 is illustrated in Figure 6b, where ν^* is found such that the maneuver aligns with the desired direction, indicated by the darker dashed arrow. The explicit values of ν^*, u^* are given in the last column of Tables 1 and 5 for eccentric and near-circular orbits respectively.

3. Substitute $\delta\boldsymbol{v}^*$, ν^* found in Steps 1 and 2 into the parameterized functions in Eq. (10). This yields $\Delta\delta(.)_x^* = \Delta\delta(.)_x(\nu^*,\delta v_t^*(\nu^*))$ and $\Delta\delta(.)_y^* = \Delta\delta(.)_y(\nu^*,\delta v_t^*(\nu^*))$, the x and y components of the vector that defines the maximum reachable distance $\Delta\delta(.)_{max} = (\Delta\delta(.)_x^{*2} + \Delta\delta(.)_y^{*2})^{1/2}$ in the direction of the desired change $\Delta\delta(.)_{des} = (\Delta\delta(.)_{x,des}, \Delta\delta(.)_{y,des})$. Equivalently, the vector points to the pseudo-state on the boundary of the convex hull defined by $||\delta\boldsymbol{v}^*|| = 1$ in the desired direction, as illustrated in Figure 6c.

4. Find δv_{min} by dividing the norm of the desired change $||\Delta\delta(.)_{des}||$ by the maximum distance $\Delta\delta(.)_{max}$, found in Step 3. This scales the reachable set such that the desired pseudo-state lies on the boundary of the convex hull, as illustrated in Figure 6d.

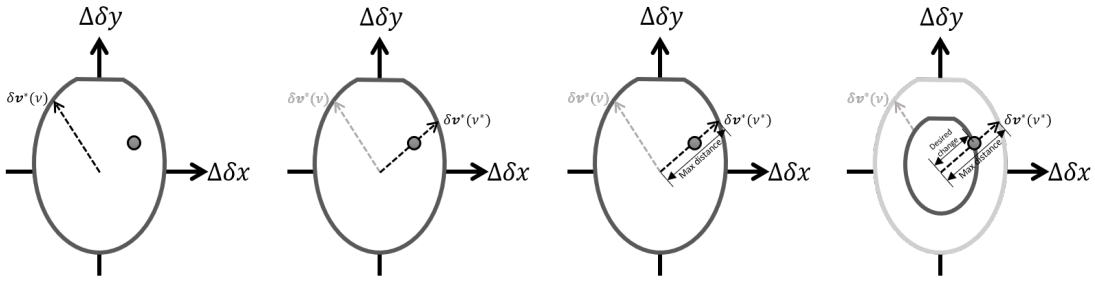

(a) Find the "best" unitary delta-v as a function of maneuver location $\delta v_t^*(\nu)$

(b) Find the maneuver location ν^* that aligns with the phase of the desired change

(c) Calculate the maximum distance along the phase direction

(d) Solve for δv_{min} as a ratio of the desired change over the maximum distance

Figure 6: Illustration of the General Methodology of the reachable delta-v minimum derivation process. Figures a-d correspond to Steps 1-4.

Example: Application of Methodology to Eccentric Chief Orbit

This example demonstrates how the General Methodology above is used to derive the dominant $\delta\boldsymbol{e}$ case in eccentric chief orbits. The example initial chief orbit is defined in terms of the classical absolute orbital elements as $\boldsymbol{\alpha}_{c,0} = [a_c, e_c, i_c, \Omega_c, \omega_c, M_c] = [16000 \text{ km}, 0.6, 8^o, 0^o, 57.3^o, 0^o]^T$. The reconfiguration time is 1.8 orbits, and the desired pseudo-state in the ROE is $a\Delta\delta\bar{\boldsymbol{\alpha}}_{des} = [-40, 830.97, 45, 120]^T$ m. This procedure is for the general case of determining $\delta v_{min,\delta\mathbf{e}}$, and the example is just demonstrative. For any reconfiguration where the chief orbit has a nonzero (and defined) argument of perigee, the reachable set $\boldsymbol{S}^*$ is rotated about the origin in the $\Delta\delta\boldsymbol{e}$ plane. To correct this rotation, let $\Delta\delta\tilde{\boldsymbol{e}}$ be the pseudo-state corrected for the rotation due to the argument of perigee, i.e., $\Delta\delta\tilde{\boldsymbol{e}} = \boldsymbol{R}^{-1}\Delta\delta\bar{\boldsymbol{e}}$ where $\boldsymbol{R}$ represents a counterclockwise rotation through ω about the origin. The parametric equations in Eq. (10) that define the boundary of $S(c,T)$ in the $\Delta\delta\tilde{\boldsymbol{e}}$ plane are the $\delta\boldsymbol{e}$ components of

$\mathbf{\Phi}(t_f, t_k)\mathbf{\Gamma}(t_k)$ rotated into the $\Delta\delta\tilde{\boldsymbol{e}}$ plane and expressed in terms of ν, and are given by

$$\begin{bmatrix}\Delta\delta\tilde{e}_x(\nu, \delta v_t(\nu))\\ \Delta\delta\tilde{e}_y(\nu, \delta v_t(\nu))\end{bmatrix} = \begin{bmatrix}\eta\sin(\nu)\sqrt{1-\delta v_t^2(\nu)} + \eta\frac{(2+e\cos(\nu))\cos(\nu)+e}{1+e\cos(\nu)}\delta v_t(\nu)\\ -\eta\cos(\nu)\sqrt{1-\delta v_t^2(\nu)} + \eta\frac{(2+e\cos(\nu))\sin(\nu)}{1+e\cos(\nu)}\delta v_t(\nu)\end{bmatrix}. \tag{11}$$

The equation for δv_t^* is derived according to Step 1 in the General Methodology above and is given by

$$\delta v_t^*(\nu) = \begin{cases} +\sqrt{\frac{1}{2} + \frac{f_1(\nu)}{2\sqrt{4+f_1(\nu)^2}}} & \text{for } \pm\Delta\delta\tilde{e}_{x,des}, \mp\Delta\delta\tilde{e}_{y,des} \\ -\sqrt{\frac{1}{2} - \frac{f_1(\nu)}{2\sqrt{4+f_1(\nu)^2}}} & \text{for } \pm\Delta\delta\tilde{e}_{x,des}, \pm\Delta\delta\tilde{e}_{y,des} \end{cases}, \text{where } \begin{matrix} f_1(\nu) = \frac{f_2(\nu)}{(1+e\cos(\nu))e\sin(\nu)} \\ f_2(\nu) = 2e^2\cos^2(\nu) + 6e\cos(\nu) + e^2 + 3 \end{matrix}. \tag{12}$$

To solve for ν^*, Eqs. (11) and (12) are substituted into Eq. (9). However, in this case, solving Eq. (9) yields two values of ν^* per orbit, so some extra considerations must be made. First, it can be shown that the arbitrary pseudo-states $\pm\Delta\delta e_x, \mp\Delta\delta e_y$ are achieved by the same δv_t^* and ν^*. The same is true for arbitrary pseudo-states $\pm\Delta\delta e_x, \pm\Delta\delta e_y$. Therefore, in place of $\Delta\delta(.)_{des}$ in Eq. (9), $\Delta\delta(.)'_{des}$ is used, given by

$$(\Delta\delta(.)'_{x,des}, \Delta\delta(.)'_{y,des}) = \begin{cases}(\Delta\delta\tilde{e}_{x,des}, \Delta\delta\tilde{e}_{y,des}) & \text{if } +\Delta\delta\tilde{e}_{y,des}\\ (-\Delta\delta\tilde{e}_{x,des}, -\Delta\delta\tilde{e}_{y,des}) & \text{if } -\Delta\delta\tilde{e}_{y,des}\end{cases} \tag{13}$$

Second, it can be shown that $S(c,t)$ briefly disconnects from the boundary of the convex hull during each orbit. By solving for the ν values that maximize the parametric $\Delta\delta\tilde{e}_y$ expression in Eq. (11), it is found that disconnection occurs at $\nu_{dis.} = \pi + \cos^{-1}(e)$ and reconnection occurs at $\nu_{re.} = \pi - \cos^{-1}(e)$. These points define the regions that contain ν^*, the maneuver locations at which $\delta v_t^*(\nu^*)$ aligns with the phase of the desired change in each orbit. Therefore,

$$\nu^* \in \begin{cases}[\pi, \nu_{dis.}] & \text{for } \pm\Delta\delta\tilde{e}_{x,des}, \pm\Delta\delta\tilde{e}_{y,des}\\ [\nu_{re.}, \pi] & \text{for } \pm\Delta\delta\tilde{e}_{x,des}, \mp\Delta\delta\tilde{e}_{y,des}\end{cases}, \tag{14}$$

which yields $\nu^* = 3.2485$ rad for the example. Following Steps 3 and 4 in the General Methodology, the general expression for reachable delta-v minimum for dominant $\delta\boldsymbol{e}$ is found in closed-form and given in Table 2. Using the last column in Table 2, $\delta v_{min,\delta\boldsymbol{e}} = 0.0249$ m/s for the example reconfiguration. Figure 7b shows the reachable set, computed with Eq. (7), for total delta-v equal to $\delta v_{min,\delta\boldsymbol{e}} = 0.0249$ m/s.

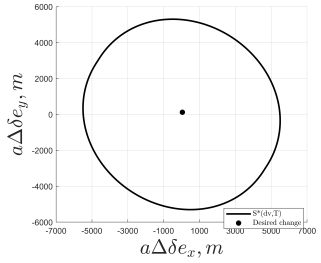

(a) S^* for arbitrary delta-v. The desired pseudo-state is not on the boundary, so this is not the optimal delta-v.

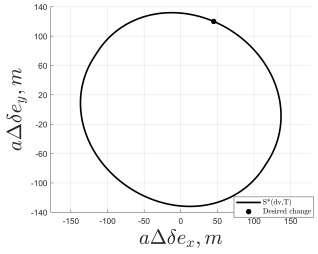

(b) $S^*(0.0249, T)$. The desired pseudo-state lies directly on the boundary, so 0.0249 m/s is the optimal delta-v.

Figure 7: Example of reachable delta-v min derivation for an eccentric orbit, dominant $\delta\boldsymbol{e}$.

The desired pseudo-state lies directly on the boundary of the convex hull, so by definition, 0.0249 m/s is the optimal delta-v for the example. Derivation of other dominance cases follows the same procedure. The results are summarized in Tables 2,3, and 4 for eccentric orbits, and 6 and 7 for near-circular orbits.

Reachable Delta-v Minimum in Eccentric Orbits

To determine the dominance case for a given reconfiguration, all independent δv_{min} must be computed and substituted into Eq. (8). The maximum δv_{min} in (8) is the dominant ROE. Table 1 lists the values of $\delta\boldsymbol{v}^*$ and ν^* found by applying Steps 1-2 in the General Methodology to each dominance case in eccentric orbits. The first column gives the region name in the case that the region proves dominant by Eq. (8). The second column gives the maneuver that achieves the maximum distance in the 2D plane as a function of the ν^* values given in the third column.

Table 1: Optimal maneuver vectors $\delta\boldsymbol{v}^*$ and optimal maneuver location ν^* for eccentric orbits

Region name	$\delta\boldsymbol{v}^*$, **(m/s)**	ν^*, **(rad)**
Dominant $\delta\boldsymbol{e}$	See Eq. (12)	Solve Eq. (9) with Eq. (14), (13)
Dominant δa	$\begin{bmatrix}0 & 1 & 0\end{bmatrix}^T$	0
Dominant $\delta\lambda$	$\begin{bmatrix}\frac{e\sin(\nu_t)}{\sqrt{e^2+2e\cos(\nu_t)+1}} & \frac{1+e\cos(\nu_t)}{\sqrt{e^2+2e\cos(\nu_t)+1}} & 0\end{bmatrix}^T$ $\begin{bmatrix}0 & 1 & 0\end{bmatrix}^T$	ν_t 0
Dominant $\delta\boldsymbol{i}$	$\begin{bmatrix}0 & 0 & 1\end{bmatrix}^T$	$\tan^{-1}\left(\frac{\Delta\delta\tilde{i}_{y,des}}{\Delta\delta\tilde{i}_{x,des}}\right)$

Note that the case of dominant $\delta\lambda$ lists two values for $\delta\boldsymbol{v}^*$, ν^*. The other maneuver location, ν_t, is the point at which the derivative of the parameterized curve (See (10)) is equal to the slope from the desired pseudo-state itself to the point of maximum norm. ν_t lies between floor$(\frac{\nu_f}{2\pi})2\pi$ and ν_f and is found by solving

$$\frac{d}{d\nu}\Delta\delta a(\nu,\delta v_t(\nu))\Big|_{\nu_t}\Big/\frac{d}{d\nu}\Delta\delta\lambda(\nu,\delta v_t(\nu))\Big|_{\nu_t}=\frac{-\Delta\delta a_0-\Delta\delta a(\nu_t,\delta v_t)(\nu)}{\Delta\delta\lambda_0-\Delta\delta\lambda(\nu_t,\delta v_t)(\nu)}. \tag{15}$$

Using Table 1 and following Steps 3-4, Tables 2, 3, and 4 present the reachable delta-v minima in all dominance cases in eccentric orbits. The second column gives the conditions on the desired ROE pseudo-state for which the expression of the reachable delta-v minimum in the fourth column applies.

Table 2: Reachable δv_{min}, eccentric chief orbits, in-plane

Region name	**Region definition**	**Max normalized effect**	δv_{min}, **(m/s)**
Dominant $\delta\boldsymbol{e}$	N/A	$\|\|\Delta\delta\tilde{\boldsymbol{e}}_{max}\|\|^2=(\Delta\delta\tilde{e}_x^*)^2+(\Delta\delta\tilde{e}_y^*)^2$ where $\Delta\delta\tilde{e}_x^*=\Delta\delta\tilde{e}_x\,(\nu^*,\delta v_t^*[\nu^*])$	$\delta v_{min,\delta\boldsymbol{e}}=na\frac{\|\|\Delta\delta\tilde{\boldsymbol{e}}_{des}\|\|}{\|\|\Delta\delta\tilde{\boldsymbol{e}}_{max}\|\|}$

The reachable delta-v minimum in the other dominance cases in eccentric orbits are derived in the same way and given in Tables 3 and 4.

Table 3: Reachable δv_{min}, eccentric chief orbits, in-plane

Region name	**Region definition**	**Max normalized effect**	δv_{min}, **(m/s)**
Dominant δa	$\Delta\delta a_{des}>0$ and $\Delta\delta\lambda_{des}<-\|\Delta\delta\lambda_{k2\pi}\|$ or $\Delta\delta a_{des}<0$ and $\Delta\delta\lambda_{des}>\|\Delta\delta\lambda_{k2\pi}\|$	$\Delta\delta a_{max}=\frac{2(e+1)}{\eta}$	$\delta v_{min,\delta a}=na\frac{\|\Delta\delta a_{des}\|}{\|\Delta\delta a_{max}\|}$
Transition region	$\Delta\delta a_{des}>0$, $-\|\Delta\delta\lambda_t\|>\Delta\delta\lambda_{des}>-\|\Delta\delta\lambda_{k2\pi}\|$ or $\Delta\delta a_{des}<0$, $\|\Delta\delta\lambda_{k2\pi}\|>\Delta\delta\lambda_{des}>\|\Delta\delta\lambda_t\|$	$\frac{\Delta\delta a_{max}=}{\frac{2\sqrt{e^2+2e\cos(\nu^*)+1}}{\eta}}$	$\delta v_{min,trans}=na\frac{\|\Delta\delta a_{des}\|}{\|\Delta\delta a_{max}\|}$
Dominant $\delta\lambda$	$\Delta\delta a_{des}>0$ and $\Delta\delta\lambda_{des}>-\|\Delta\delta\lambda_t\|$ or $\Delta\delta a_{des}<0$ and $\Delta\delta\lambda_{des}<\|\Delta\delta\lambda_t\|$ or large $\Delta\delta\lambda$	N/A	$\delta v_{min,\delta\lambda}=na\left\|\frac{m\Delta\delta\lambda_{des}-\Delta\delta a_{des}}{m\Delta\delta\lambda_t-\Delta\delta a_t}\right\|$ where $m=\frac{-\|\Delta\delta a_0\|-\Delta\delta a_t}{\|\Delta\delta\lambda_0\|-\Delta\delta\lambda_t}$
Extended regions	Region 1 if $\Delta\delta\lambda_{des}<\delta v_{min,\delta\lambda}\Delta\delta\lambda_f$	N/A	$\delta v_{min}=na\frac{\Delta\delta a_{des}-m_1\Delta\delta\lambda_{des}}{m_1\|\Delta\delta\lambda_{k2\pi}\|+\|\Delta\delta a_{k2\pi}\|}$ where $m_1=\frac{\|\Delta\delta a_f\|-\|\Delta\delta a_{k2\pi}\|}{\|\Delta\delta\lambda_f\|+\|\Delta\delta\lambda_{k2\pi}\|}$
	Region 2 if $\Delta\delta\lambda_{des}>\delta v_{min,\delta\lambda}\Delta\delta\lambda_f$	N/A	$\delta v_{min}=na\frac{\Delta\delta a_{des}-m_2\Delta\delta\lambda_{des}}{m_2\|\Delta\delta\lambda_f\|+\|\Delta\delta a_f\|}$ where $m_2=\frac{-\|\Delta\delta a_0\|-\|\Delta\delta a_f\|}{\|\Delta\delta\lambda_0\|-\|\Delta\delta\lambda_f\|}$
	Exists if $\|(\|\Delta\delta a_f\|-\Delta\delta a_t)/(\|\Delta\delta\lambda_f\|-\Delta\delta\lambda_t)\|<\|(-\|\Delta\delta a_0\|-\Delta\delta a_t)/(\|\Delta\delta\lambda_0\|-\Delta\delta\lambda_t)\|$		

As in Eq. (11), the parametric equations in the $\Delta\delta a, \Delta\delta\lambda$ plane in Eq. (10) are the $\delta a, \delta\lambda$ components of $\mathbf{\Phi}(t_f, t_k)\mathbf{\Gamma}(t_k)$, given by

$$\begin{bmatrix}\Delta\delta\lambda(\nu, \delta v_t(\nu))\\ \Delta\delta a(\nu, \delta v_t(\nu))\end{bmatrix} = \begin{bmatrix}\left(-\frac{2\eta^2}{1+e\cos(\nu)} - \frac{3}{\eta}\Delta M e\sin(\nu)\right)\sqrt{1-\delta v_t^2(\nu)} + -\frac{3}{\eta}\Delta M\left(1+e\cos(\nu)\right)\delta v_t(\nu)\\ \frac{2}{\eta}e\sin(\nu)\sqrt{1-\delta v_t^2(\nu)} + \frac{2}{\eta}\left(1+e\cos(\nu)\right)\delta v_t(\nu).\end{bmatrix} \tag{16}$$

In Table 3, the states used to compute $\delta v_{min,\delta\lambda}$ are

$$\begin{array}{l}\Delta\delta\lambda_{k2\pi} : \delta\boldsymbol{v} = \begin{bmatrix}0 & \delta v_{min,\delta a} & 0\end{bmatrix}^T \text{ at } \nu = \text{floor}(\frac{\nu_f}{2\pi})2\pi \text{ and}\\ \Delta\delta\lambda_t, \Delta\delta a_t : \delta\boldsymbol{v} = \frac{\delta v_{min,\delta a}}{\sqrt{e^2+2e\cos(\nu_t)+1}}\begin{bmatrix}e\sin(\nu_t) & 1+e\cos(\nu_t) & 0\end{bmatrix}^T \text{ at } \nu = \nu_t \text{ (Eq. (15))}.\end{array} \tag{17}$$

Table 4 presents the reachable delta-v minimum for out-of-plane reconfigurations in eccentric orbits. Just as in the $\Delta\delta\boldsymbol{e}$ plane, the reachable set $\boldsymbol{S}^*$ is rotated about the origin for any reconfiguration where the chief has a nonzero (and defined) argument of perigee. The parametric equations in the $\Delta\delta\boldsymbol{i}$ plane in Eq. (10) are rotated into the $\Delta\delta\tilde{\boldsymbol{i}}$ plane using the same rotation matrix as in the $\Delta\delta\tilde{\boldsymbol{e}}$ case, and are given by

$$\begin{bmatrix}\Delta\delta\tilde{i}_x(\nu, \delta v_n(\nu))\\ \Delta\delta\tilde{i}_y(\nu, \delta v_n(\nu))\end{bmatrix} = \frac{\eta}{1+e\cos(\nu)}\begin{bmatrix}\cos(\nu)\\ \sin(\nu)\end{bmatrix}\delta v_n(\nu). \tag{18}$$

As in the dominant $\delta\boldsymbol{e}$ case and shown in Figure 3c, the reachable set $S(c,t)$ briefly disconnects from the boundary of the convex hull during each orbit. By solving for the ν values that maximize the parametric $\Delta\delta\tilde{i}_y$ expression in Eq. (18), it is found that disconnection occurs at $\nu_{dis.} = \pi + \cos^{-1}(e)$ and reconnection occurs at $\nu_{re.} = \pi - \cos^{-1}(e)$, the same ν locations as in the $\Delta\delta\tilde{\boldsymbol{e}}$ case. Reconfigurations whose desired pseudo-state lies in the disconnected region require a slightly different formulation of the reachable delta-v, given in the second row of Table 4. In Table 4, $\nu^* = \tan^{-1}(\frac{\Delta\delta\tilde{i}_y}{\Delta\delta\tilde{i}_x})$, the phase of the rotated desired change.

Table 4: Reachable δv_{min}, eccentric chief orbits, out-of-plane

Region name	**Region definition**	**Max normalized effect**	δv_{min}, **(m/s)**
Dominant $\delta\boldsymbol{i}$	$\nu' = \nu^*$ or $\nu' = \nu^* + \pi \in (\nu_{re}, \nu_{dis})$	$\|\|\Delta\delta\tilde{\boldsymbol{i}}_{max}\|\| = \frac{\eta}{1+e\cos(\nu')}$	$na\frac{\|\|\Delta\delta\tilde{\boldsymbol{i}}_{des}\|\|}{\|\|\Delta\delta\tilde{\boldsymbol{i}}_{max}\|\|}$
	$\nu' = \nu^*$ and $\nu' = \nu^* + \pi \notin (\nu_{re}, \nu_{dis})$	$\|\Delta\delta\tilde{i}_{y,max}\| = \frac{\sin(\nu_{re.})\eta}{1+e\cos(\nu_{re.})}$	$na\frac{\|\Delta\delta\tilde{i}_{y,des}\|}{\|\Delta\delta\tilde{i}_{y,max}\|}$

Reachable Delta-v Minimum in Near-Circular Orbits

Table 5 lists the values of $\delta\boldsymbol{v}^*$ and ν^* found by applying Steps 1-2 in the General Methodology to each dominance case in near-circular orbits. As in eccentric orbits, the dominant $\delta\lambda$ case requires two maneuvers.

Table 5: Optimal maneuver vectors $\delta\boldsymbol{v}^*$ and optimal maneuver location u^* for near-circular orbits

Region name	$\delta\boldsymbol{v}^*$, **(m/s)**	u^***, (rad)**
Dominant $\delta\boldsymbol{e}$ *Dominant* δa	$\begin{bmatrix}0 & 1 & 0\end{bmatrix}^T$	Anywhere
Dominant $\delta\lambda$	$\begin{bmatrix}0 & 1 & 0\end{bmatrix}^T$ $\begin{bmatrix}0 & 1 & 0\end{bmatrix}^T$	0 u_f
Dominant $\delta\boldsymbol{i}$	$\begin{bmatrix}0 & 0 & 1\end{bmatrix}^T$	Anywhere

The boundary of the convex hull in the $\Delta\delta\boldsymbol{e}$ plane is reachable by a tangential maneuver of magnitude one anywhere in the orbit, so for calculation of the reachable delta-v minimum, the value of u^* does not matter. The same is true for the $\Delta\delta a$ convex hull. However, as shown in the next section, maneuvers are performed at specific u (u_{opt}) to achieve a reconfiguration with delta-v equal to the reachable delta-v minimum. For zero eccentricity,

there are fewer dominance cases and simpler expressions for the reachable delta-v minima, given by Tables 6 and 7.

Table 6: Reachable δv_{min}, near-circular chief orbits, in-plane

Region name	**Region definition**	**Max normalized effect**	δv_{min} **(m/s)**
Dominant $\delta\boldsymbol{e}$	N/A	$\|\|\Delta\delta\boldsymbol{e}_{max}\|\| = 2$	$\delta v_{min,\delta\boldsymbol{e}} = na\frac{\|\|\Delta\delta\tilde{\boldsymbol{e}}_{des}\|\|}{\|\|\Delta\delta\boldsymbol{e}_{max}\|\|}$
Dominant δa	$\Delta\delta\bar{a}_{des} > 0, \Delta\delta\bar{\lambda}_{des} < 0$ or $\Delta\delta\bar{a}_{des} < 0, \Delta\delta\bar{\lambda}_{des} > 0$	$\|\Delta\delta a_{max}\| = 2$	$\delta v_{min,\delta a} = na\frac{\|\Delta\delta a_{des}\|}{\|\Delta\delta a_{max}\|}$
Dominant $\delta\lambda$	$\Delta\delta\bar{a}_{des} > 0, \Delta\delta\bar{\lambda}_{des} > 0$ or $\Delta\delta\bar{a}_{des} < 0, \Delta\delta\bar{\lambda}_{des} < 0$ or large $\Delta\delta\lambda_{des}$	N/A	$\delta v_{min,\delta\lambda} = na\left\|\frac{m\Delta\delta\lambda_{des} - \Delta\delta a_{des}}{-\|\Delta\delta a_0\|}\right\|$ where $m = \frac{-2\|\Delta\delta a_0\|}{\|\Delta\delta\lambda_0\|}$

In Table 6, $\Delta\delta\lambda_0$, $\Delta\delta a_0$ refer to the values of the relative mean longitude and relative semi-major axis found by applying the maneuver in the second row of Table 5 at $u = 0$.

Table 7: Reachable δv_{min}, near-circular chief orbits, out-of-plane

Region name	**Region definition**	**Max normalized effect**	δv_{min}**, (m/s)**
Dominant $\delta\boldsymbol{i}$	N/A	$\|\|\Delta\delta\boldsymbol{i}_{max}\|\| \approx 1$	$\delta v_{min,\delta\boldsymbol{i}} = na\frac{\|\|\Delta\delta\bar{\boldsymbol{i}}_{des}\|\|}{\|\|\Delta\delta\boldsymbol{i}_{max}\|\|}$

Notice that in Table 7, $||\Delta\delta\boldsymbol{i}_{max}|| \approx 1$. This is because J_2 causes a very slight warping of a perfect circle of radius one. However, this effect is negligible in calculating the reachable δv_{min}. The next section presents the explicit closed-form maneuver schemes that accomplish a desired reconfiguration with a fuel cost equal to the reachable delta-v minimum derived in this section.

CLOSED-FORM MANEUVER SCHEMES

This section first presents the general methodology to calculate an optimal maneuver scheme, then gives the explicit closed-form solutions for multiple relevant cases.

General Methodology

Given an initial chief orbit $\boldsymbol{\alpha}_{c,0}$, a desired pseudo-state $\Delta\delta\bar{\boldsymbol{\alpha}}_{des}$, and a reconfiguration time T, the general methodology to calculate closed-form, optimal maneuver schemes is given step-by-step as follows.

1. Determine the dominance case and reachable delta-v minimum. The dominance case and corresponding reachable delta-v minimum are found by computing all independent δv_{min} using Tables 1-4 for eccentric orbits or Tables 5-7 for near-circular orbits and substituting them into Eq. (8).

2. Find the set of optimal maneuver locations ν_{opt} or u_{opt} (or equivalently, T_{opt}). The optimization problem in Eq. (2) is computationally intractable for many linear time-variant systems. As Koenig[15] details, this problem is remedied by solving the dual of Eq. (2), which is

$$\begin{aligned} &\text{Maximize: } \delta v \\ &\text{subject to: } \max_{\boldsymbol{z}\in S^*(\delta v,T)} \boldsymbol{\lambda}^T\boldsymbol{z} \leq \boldsymbol{\lambda}^T\Delta\delta\bar{\boldsymbol{\alpha}}_{des}, \end{aligned} \tag{19}$$

where $\boldsymbol{\lambda}$ is the normal vector of a supporting hyperplane of $S^*(\delta v, T)$, $L(\Delta\delta\bar{\boldsymbol{\alpha}}_{des}, \boldsymbol{\lambda})$ (or L), which contains the desired pseudo-state $\Delta\delta\bar{\boldsymbol{\alpha}}_{des}$. It is not necessary to solve the optimization problem itself in this paper because the ROE state representation yields geometrically simple reachable sets. However, Koenig's analysis yields properties that help provide some geometric intuition in solving Eq. (2). Once the reachable delta-v minimum is known for a given reconfiguration, the projection of L in the dominant 2D plane is the line that passes through the desired pseudo-state and is tangent to $S^*(\delta v_{min}, T)$. Therefore, every point in the intersection between L

and $S^*(\delta v_{min}, T)$ is in the boundary of $S^*(\delta v_{min}, T)$, and the desired pseudo-state must be in $L \cap S^*(\delta v_{min}, T)$ as well. By definition of the convex hull in Eq. (7), it is possible to find a convex combination of points in $L \cap S^*(\delta v_{min}, T)$ that achieves the desired reconfiguration with cost equal to δv_{min}. Therefore, a set of optimal maneuver times T_{opt} must be found such that the optimality condition in the dominant plane is satisfied. In other words, T_{opt} is the set of all times in T at which L can be reached with a single maneuver, and is found by determining where $S(c,t)$ (Eq. (5)) intersects the boundary of $S^*(c,T)$.

3. Generate nested reachable sets using T_{opt} from the previous step. The nested reachable set $S_n^*(\delta v_{min}, T_{opt})$ is calculated using Eq. (7) for only the times in T_{opt}, with $\delta \boldsymbol{v}$ equal to $\delta \boldsymbol{v}^*$ (Tables 1,5) scaled by δv_{min}. Because T_{opt} is a subset of T, $S_n^*(\delta v_{min}, T_{opt})$ is a subset of $S(\delta v_{min}, T)$. As noted in the previous section, the desired pseudo-state projected in the non-dominant plane must lie in the nested reachable set in order for the reachable delta-v minimum to be equal to the values in Tables 2-4, 6-7. Figures 8 and 9 illustrate S_n (shaded region or point), where the desired pseudo-state must lie in the non-dominant plane for a closed-form solution using δv_{min} to exist, for each dominance case.

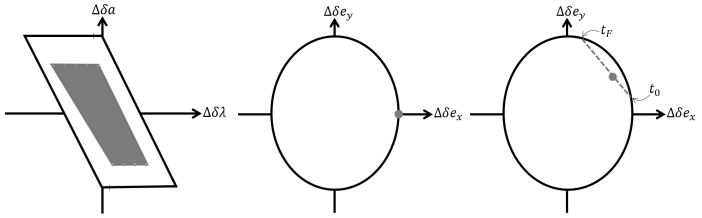

(a) Dominant $\delta \boldsymbol{e}$ (b) Dominant δa (c) Dominant $\delta \lambda$

Figure 8: In eccentric orbits, the desired pseudo-state must lie in the shaded nested reachable set (S_n^*) for the full reconfiguration to be achievable.

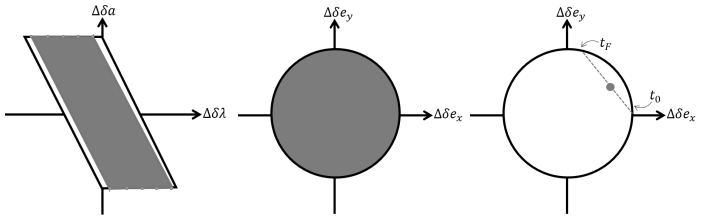

(a) Dominant $\delta \boldsymbol{e}$ (b) Dominant δa (c) Dominant $\delta \lambda$

Figure 9: In near-circular orbits, the desired pseudo-state must lie in the shaded nested reachable set (S_n^*) for the full reconfiguration to be achievable.

The biggest difference between the nested reachable sets in near-circular and eccentric orbits is in the dominant δa case. In near-circular orbits, $\Delta \delta a$ is independent of the maneuver location, so T_{opt} is an infinite set and $S_n^* = S^*$. In contrast, $\Delta \delta a$ is dependent on the maneuver location in eccentric orbits, which means that there is a finite set of times in T_{opt} (multiples of 2π). Therefore, the only pseudo-states that are reachable occur at maneuver locations that are multiples of 2π, so S_n^* is a single point at the boundary of S^* on the $\Delta \delta e_x$-axis (See Figure 8b). In addition, as shown in Figure 8c and 9c, for dominant $\delta \lambda$, S_n^* is the pseudo-state that lies on the segment (dashed line) connecting the pseudo-states at the two times in T_{opt}, t_0 at the start of the reconfiguration, and t_f at the end.

4. Satisfy constraints. Each dominance case has a set of constraints that must be satisfied in order for (1) a closed-form solution to exist and (2) the closed-form solution to be energy-optimal. A Type 1 constraint requires the desired pseudo-state to be inside or on the boundary of the nested reachable set, and a Type 2 constraint ensures that the total cost of the maneuver scheme is equal to δv_{min}, i.e., $\sum_i^k ||\delta \boldsymbol{v}_i|| = \delta v_{min}$. The third column of Tables 9 and 11 summarizes the Type 1 constraints for all cases in eccentric orbits and near-circular orbits, respectively. The set of constraints translates to a linear system to be solved for the maneuver magnitudes,

$c_1, c_2, ..., c_p$. After solving the linear system, the best solution can be found by choosing the set of maneuvers that satisfies any additional constraints, such as collision avoidance or maneuver exclusion windows. Note that the number of required maneuvers in Column 3 of Tables 9 and 11 is not arbitrary. The size of the state and the location of the desired pseudo-state drive the number of required maneuvers. To control a single 2D state, such as the out-of-plane ROE, one maneuver is required if the desired pseudo-state lies in both S and S*, and two maneuvers are required if the desired pseudo-states lies just in S*. This is apparent in the definition of S and S* in Eqs. (6) and (7). To control a 4D state, such as the in-plane ROE, more maneuvers are required to satisfy the constraints of achieving the desired pseudo-state in each of the four dimensions.

5. Solve linear system. At this point, only the maneuver magnitudes are unknown. Sets of p maneuver times (given in the second column of Table 9 or 11) and corresponding pseudo-states in S_n ($\Delta\delta a_k$, $\Delta\delta\lambda_k$, $\Delta\delta e_{x,k}$, $\Delta\delta e_{y,k}$ for $k = 1, .., p$) must be chosen such that the Type 1 constraints in column three of Table 9 or Table 11 are satisfied. The Type 2 constraint always translates to $\sum_{k=1}^{p} c_i = 1$ in the linear system. The resulting linear system is of the form $\boldsymbol{Ac} = \boldsymbol{b}$ with unknown coefficients $\boldsymbol{c}$. Since the determinant is always non-null based on the choice of maneuvers in S_n, the linear system can be solved by $\boldsymbol{c} = \boldsymbol{A}^{-1}\boldsymbol{b}$.

Closed-form Solutions in Eccentric Orbits

This section gives explicit closed-form maneuver schemes in eccentric orbits, which result from application of the General Methodology described in the previous section. Table 8 gives the optimal maneuver $\delta\boldsymbol{v}^*$ (column 2) and set of optimal maneuver locations ν_{opt} (column 3) for relevant reconfiguration cases in eccentric orbits. The difference between column 2 in Table 8 and column 2 of Tables 1 and 5 is that Tables 1 and 5 were only concerned with finding the scaling factor (δv_{min}) on the reachable set such that the desired pseudo-state was on the boundary of the convex hull. In contrast, Table 8 lists the specific maneuver locations required to achieve the desired reconfiguration with delta-v equal to δv_{min}.

In the $\Delta\delta\boldsymbol{e}$ plane, L is only reachable when $S(c,t)$ aligns with the desired direction, because L is tangent to the reachable set only at the desired pseudo-state. Because $S(c,t)$ is periodic in the $\Delta\delta\boldsymbol{e}$ plane, it will align with the desired direction every half orbit, at so-called $\nu_{opt,1}$ and $\nu_{opt,2}$. The first value, $\nu_{opt,1}$, is equal to ν^*, which was found by substituting Eqs. (11)-(14) into Eq. (9). The second value, $\nu_{opt,2}$, is found using the unused definition of δv_t^* and ν^* in Eqs. (12) and (14), respectively. The explicit values in ν_{opt} are integer multiples of 2π away from $\nu_{opt,1}$ or $\nu_{opt,2}$. This is summarized in the last column of row 1 in Table 8.

Table 8: Optimal maneuver vectors $\delta\boldsymbol{v}^*$ and set of optimal maneuver times T_{opt} for eccentric orbits

Region	$\delta\boldsymbol{v}^*$**, (m/s)**	ν_{opt}**, (rad)**
Dominant $\delta\boldsymbol{e}$	See Eq. (12)	$\nu_{opt,1} + k\pi$, $k = \text{floor}(\frac{\nu_f - \nu_{opt,1}}{2\pi})$ $\nu_{opt,2} + k\pi$, $k = \text{floor}(\frac{\nu_f - \nu_{opt,2}}{2\pi})$
Dominant $\delta\boldsymbol{i}$		
$\nu' = \nu^* \in (\nu_{re}, \nu_{dis})$	$\begin{bmatrix}0 & 0 & +\delta v_{min,\delta\boldsymbol{i}}\end{bmatrix}^T$	$\nu' + k2\pi$, $k = \text{floor}(\frac{\nu_f - \nu'}{2\pi})$
$\nu' = \nu^* + \pi \in (\nu_{re}, \nu_{dis})$	$\begin{bmatrix}0 & 0 & -\delta v_{min,\delta\boldsymbol{i}}\end{bmatrix}^T$	$\nu' + k2\pi$, $k = \text{floor}(\frac{\nu_f - \nu'}{2\pi})$
Else	At $\nu_{re} + k2\pi$, $\begin{bmatrix}0 & 0 & +\delta v_{min,\delta\boldsymbol{i}}\end{bmatrix}^T$ At $\nu_{dis} + k2\pi$, $\begin{bmatrix}0 & 0 & -\delta v_{min,\delta\boldsymbol{i}}\end{bmatrix}^T$	$\nu_{re} + k2\pi$ $\nu_{dis} + k2\pi$, $k = \text{floor}(\frac{\nu_f - \nu_{dis}}{2\pi})$

After computing the optimal times and maneuvers using Table 8, the nested reachable set is generated according to Step 3 of the General Methodology described in the previous section. Then, according to Step 4, a subset of maneuvers is chosen from S_n such that it satisfies a set of constraints. Table 9 gives the specific constraints that must be satisfied (column 3) and the corresponding linear system (column 4) to solve in Steps 4-5 of the General Methodology. In Table 9, the subscript max (min) refers to the largest (smallest) value of that ROE in the nested reachable set for the chosen set of 3 maneuvers.

Table 9: Closed-form maneuver scheme constraints in eccentric orbits

Region	**# of Maneuvers**	**Constraints (Type 1)**	**Linear System**
Dominant $\delta\boldsymbol{e}$	3	$\begin{matrix} a\Delta\delta a_{max} \geq a\Delta\delta a_{des} \geq a\Delta\delta a_{min} \\ a\Delta\delta\lambda_{max} \geq a\Delta\delta\lambda_{des} \geq a\Delta\delta\lambda_{min} \end{matrix}$ *	$\begin{matrix} \sum_{i=1}^{3} c_i = 1 \\ \sum_{i=1}^{3} c_i a\Delta\delta a_i = a\Delta\delta\bar{a}_{des} \\ \sum_{i=1}^{3} c_i a\Delta\delta\lambda_i = a\Delta\delta\bar{\lambda}_{des} \end{matrix}$
Dominant $\Delta\delta\boldsymbol{i}$			
$\nu' = \nu^* \in (\nu_{re}, \nu_{dis})$	1	N/A	$c_1 = 1$
$\nu' = \nu^* + \pi \in (\nu_{re}, \nu_{dis})$	1	N/A	$c_1 = 1$
Else	2	N/A	$\begin{matrix} \sum_{i=1}^{2} c_i a\Delta\delta\tilde{i}_x = a\Delta\delta\tilde{i}_{x,des} \\ \sum_{i=1}^{2} c_i a\Delta\delta\tilde{i}_y = a\Delta\delta\tilde{i}_{y,des} \end{matrix}$

Closed-form Solutions in Near-Circular Orbits

This section gives explicit closed-form maneuver schemes in near-circular orbits perturbed by J_2. The extra drift in $\delta\boldsymbol{e}$ induced by maneuvers can be compensated by slightly offsetting maneuver times. First, the rotation rate of the $\Delta\delta\boldsymbol{e}$ vector, $\dot{\varphi}$, is found by computing

$$\dot{\varphi} = \frac{d}{dt}\tan^{-1}\frac{\Delta\delta e_y}{\Delta\delta e_x} = \frac{\frac{d}{dt}(\Delta\delta e_y)\Delta\delta e_x - \frac{d}{dt}(\Delta\delta e_x)\Delta\delta e_y}{\Delta\delta e_x^2 + \Delta\delta e_y^2} = -\dot{\omega} + (n + \kappa(\eta P + Q)) = n + \kappa\eta P, \tag{20}$$

using the constants in Eq. (33). Then, the initial angle of the vector in the $\Delta\delta\boldsymbol{e}$ plane is found to be $\varphi_0 = \kappa Q t_f + \omega_{c,0}$. Finally, the expression for the optimal maneuver times in the dominant $\delta\boldsymbol{e}$ and dominant δa cases in near-circular orbits is given by

$$T_{opt} = \frac{(\tan^{-1}(\frac{\Delta\delta\bar{e}_{y,des}}{\Delta\delta\bar{e}_{x,des}}) + m\pi) - (\kappa Q t_f + \omega_0)}{\dot{\varphi}} + k_i\frac{\pi}{\dot{\varphi}}, \tag{21}$$

where $m\pi$ is added until $(\tan^{-1}(\frac{\Delta\delta\bar{e}_{y,des}}{\Delta\delta\bar{e}_{x,des}}) + m\pi) > (\kappa Q t_f + \omega_0)$ and $k_i \in \mathbb{N}$ including zero. The relative inclination vector also experiences a drift due to J_2 but the rotation rate of $\Delta\delta\boldsymbol{i}$ is a function of the maneuver location, so it cannot be used to compensate the optimal maneuver times as in Eq. (21) above. Instead, considering J_2's effect on each individual maneuver, T_{opt} is given by

$$T_{opt} = \frac{\tan^{-1}(\frac{\Delta\delta\bar{i}_y}{\Delta\delta\bar{i}_x}) + m\pi + k_i\pi - \omega_0}{n + \kappa(\eta P + Q)}, \tag{22}$$

where $m\pi$ is added until $(\tan^{-1}(\frac{\Delta\delta\bar{i}_{y,des}}{\Delta\delta\bar{i}_{x,des}}) + m\pi) > \omega_0$ and $k_i \in \mathbb{N}$ including zero.

Table 10: Optimal maneuver vectors $\delta\boldsymbol{v}^*$ and set of optimal maneuver times T_{opt} for near-circular orbits

Region	$\delta\boldsymbol{v}^*$, (m/s)	T_{opt}, (s)
Dominant δa	$\Delta\delta a > 0:\ \delta\boldsymbol{v}^* = \begin{bmatrix}0 & +\delta v_{min,\delta a} & 0\end{bmatrix}^T$ for all i $\Delta\delta a < 0:\ \delta\boldsymbol{v}^* = \begin{bmatrix}0 & -\delta v_{min,\delta a} & 0\end{bmatrix}^T$ for all i	See Eq. (21)
Dominant $\delta\boldsymbol{e}$	$k_i + m$ even : $\delta\boldsymbol{v}_i^* = \begin{bmatrix}0 & +\delta v_{min,\delta\boldsymbol{e}} & 0\end{bmatrix}^T$ $k_i + m$ odd : $\delta\boldsymbol{v}_i^* = \begin{bmatrix}0 & -\delta v_{min,\delta\boldsymbol{e}} & 0\end{bmatrix}^T$	See Eq. (21)
Dominant $\delta\boldsymbol{i}$	$k_i + m$ even : $\delta\boldsymbol{v}_i^* = \begin{bmatrix}0 & 0 & +\delta v_{min,\delta\boldsymbol{i}}\end{bmatrix}^T$ $k_i + m$ odd : $\delta\boldsymbol{v}_i^* = \begin{bmatrix}0 & 0 & -\delta v_{min,\delta\boldsymbol{i}}\end{bmatrix}^T$	See Eq. (22)

In Table 10, i refers to the time in T_{opt} calculated with $k_i \in \mathbb{N}$ in Eq. (21) or (22). As in eccentric orbits, the

nested reachable set is generated using Eq. (7) with the optimal times and maneuvers from Table 10 as inputs, and maneuvers are chosen from that set according to a set of constraints given in column 3 of Table 11. Then the corresponding linear system in column 4 of Table 11 is solved.

Table 11: Closed-form maneuver scheme constraints in near-circular orbits

Region	**# of Maneuvers**	**Constraints (Type 1)**	**Linear System**
Dominant δa	3	$a\Delta\delta\lambda_{max} \geq a\Delta\delta\bar{\lambda}_{des} \geq a\Delta\delta\lambda_{min}$ Not all odd or even k_i	$\sum_{i=1}^{3} c_i = 1$ $\sum_{i=1}^{3} c_i a\Delta\delta\lambda_i = a\Delta\delta\bar{\lambda}_{des}$ $\sum_{i=1}^{3} \pm c_i a\|\|\Delta\delta\boldsymbol{e}_i\|\| = a\|\|\Delta\delta\bar{\boldsymbol{e}}_{des}\|\|$
Dominant $\delta\boldsymbol{e}$	3	$a\Delta\delta a_{max} \geq a\Delta\delta\bar{a}_{des} \geq a\Delta\delta a_{min}$ $a\Delta\delta\lambda_{max} \geq a\Delta\delta\bar{\lambda}_{des} \geq a\Delta\delta\lambda_{min}$	$\sum_{i=1}^{3} c_i = 1$ $\sum_{i=1}^{3} c_i a\Delta\delta\lambda_i = a\Delta\delta\bar{\lambda}_{des}$ $\sum_{i=1}^{3} c_i a\Delta\delta a_i = a\Delta\delta\bar{a}_{des}$
Dominant $\delta\boldsymbol{i}$	1	N/A	$c_1 = 1$

For the dominant $\Delta\delta a$ case in Table 11 column 3, if $\Delta\delta a_{des} > 0$, positive $||\Delta\delta\boldsymbol{e}||_i$ is used if the phase of the desired change and u_m both correspond to $\Delta\delta e_y > 0$ or to $\Delta\delta e_y < 0$. If $\Delta\delta a_{des} < 0$, negative $||\Delta\delta\boldsymbol{e}||_i$ is used if the phase of the desired change and u_m both correspond to $\Delta\delta e_y > 0$ or to $\Delta\delta e_y < 0$.

The use of three maneuvers in the dominant δa algorithm in near-circular orbits restricts the nested reachable set slightly. Therefore, there may be values of $\Delta\delta\bar{\lambda}_{des}$ that lie inside the nested reachable set but cannot be reached with the algorithm in Table 11. See Appendix C for details. Because the nested reachable sets are restricted to single points in the non-dominant plane (Figures 8 and 9), solutions for the dominant δa case in eccentric orbits and the dominant $\delta\lambda$ case in near-circular orbits and eccentric orbits are not included in the tables in this section, but closed-form globally-optimal solutions for the case where only the desired change in the dominant plane is important are given in Appendix B.

The tables in this section present a few important and relevant cases, but the methodology above is general. Using the validation methods in the next section, it can be confirmed that a maneuver scheme computed using the tables presented here does achieve the desired reconfiguration with minimum cost.

VALIDATION

The new closed-form maneuver schemes are validated in this section. Numerical integration of the GVE is used to verify that the control solutions achieve the desired formation reconfiguration. In addition, the optimality of the maneuver schemes is confirmed by comparing the computed reachable delta-v to the output of Koenig et al.'s numerical algorithm.[15] The numerical integration architecture is as follows. Reconfiguration parameters ($\delta\boldsymbol{\alpha}_0$, $\boldsymbol{\alpha}_{c,0}$, and T) and maneuver scheme (t_k, $\delta\boldsymbol{v}_k$ for $k = 1, ..., p$) are provided as inputs. First, the initial mean deputy orbital elements, $\boldsymbol{\alpha}_{d,0}$, are extracted from $\delta\boldsymbol{\alpha}_0$ and $\boldsymbol{\alpha}_{c,0}$ using the nonlinear relationships in Eq. (3). The chief and deputy orbital elements are both transformed to osculating orbital elements using Brouwer's transformation[21] and simultaneously propagated forward by numerical integration of the GVE including J_2 effects. At the time of a maneuver, the maneuver is added as an instantaneous change in the relative velocity with no change in position. After the maneuver, the propagator is reinitialized with the same osculating chief orbital elements and the new osculating deputy orbital elements resulting from the applied maneuver. This process is repeated until the last maneuver, and then both sets of orbital elements are propagated to the end of the reconfiguration time. The final osculating orbital elements are converted first back into mean orbital elements, then back to ROE for comparison to the desired final ROE. This process is shown in compact block diagram form in Figure 10.

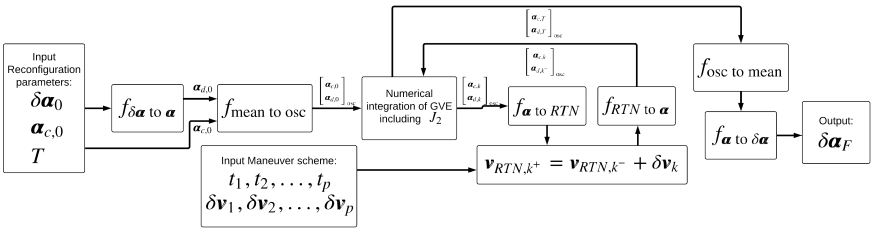

Figure 10: Simulation architecture for numerical integration of the GVE including maneuvers.

The second validation method uses Koenig et al.'s algorithm to confirm optimality. The optimization problem in Eq. (2) is solved in order to maximize the delta-v cost subject to the constraint that the desired reconfiguration cannot be reached at a lesser cost. This is equivalent to maximizing the cost to reach a supporting hyperplane L which contains the target. The hyperplane is defined by a normal vector $\boldsymbol{\lambda}$ tangent to the boundary of the convex hull at the desired pseudo-state. As Koenig shows,[15] a lower bound on the minimum reconfiguration cost can be found using an algorithm which iteratively refines $\boldsymbol{\lambda}$ by adding and removing candidate maneuver times in order to improve the cost. Figure 11 is a graphical overview of the algorithm. Once the lower bound, δv_{lb}, has been computed numerically using Koenig's algorithm, it will be compared to the reachable minimum delta-v, δv_{min}, derived in this paper to confirm global optimality.

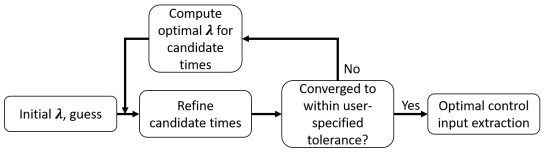

Figure 11: Algorithm to iteratively compute lower bound on minimum reconfiguration cost.[15]

Two example reconfigurations are defined to demonstrate the new closed-form maneuver schemes in realistic mission scenarios. Test 1 applies the maneuver schemes and reachable delta-v minimum analysis to a required in-plane reconfiguration in NASA's ongoing Magnetospheric Multiscale (MMS) Mission,[24] and Test 2 evaluates the out-of-plane control solutions for a required reconfiguration in the mDOT mission.[25,26]

Results

Each example in this section will include an error report and plots that show the evolution of the ROE in the presence of impulsive maneuvers.

Test 1: MMS Mission swarm reconfiguration in unperturbed, highly eccentric chief orbit, dominant $||\Delta\delta\boldsymbol{e}||$. NASA's MMS mission seeks to improve humanity's understanding of how magnetic reconnection works in the universe by studying Earth's magnetosphere with a swarm of four satellites in a tetrahedral formation in a highly eccentric orbit.[24,27] The two year mission has two distinct phases: Phase 1, where MMS will fly through the boundary where Earth's magnetic field lines up with the Sun's, and Phase 2, where MMS will fly through reconnection sites in Earth's magnetic tail.[24] Phase 1 required reconfiguration of the swarm between tetrahedral formations with side lengths of 10-160 km with zero along-track drift.[28] Using available data, the reconfiguration in this example transfers one of the satellites in the swarm from its spot in a 10 km formation to its spot in a 60 km formation. Phase 1 of the MMS mission included an interim reconfiguration from 10 km to 25 km and from 25 km to 60 km, but this data was unavailable. The initial[27] and final[29] mean orbital elements for reconfiguration of one of the three deputy satellites are given by

$$\begin{aligned}\boldsymbol{\alpha}_{d,0} &= \begin{bmatrix}42095.7\text{ km} & 0.81799342 & 27.801283^o & 359.98943^o & 15.002286^o & 180.00303^o\end{bmatrix}^T,\\ \boldsymbol{\alpha}_{d,f} &= \begin{bmatrix}42095.7\text{ km} & 0.81749305 & 27.805202^o & 359.94611^o & 15.002637^o & 180.01889^o\end{bmatrix}^T,\end{aligned} \tag{23}$$

and the corresponding reconfiguration parameters are

$$\begin{aligned}
\boldsymbol{\alpha}_{c,0} &= \begin{bmatrix}42095.7\text{ km} & 0.81818 & 27.8^o & 0^o & 15^o & 180^o\end{bmatrix}^T \\
\delta\bar{\boldsymbol{\alpha}}_0 &= \begin{bmatrix}0 & -758.3 & -7942.0 & -706.4 & 942.6 & -3621.9\end{bmatrix}^T\text{ m} \\
\delta\bar{\boldsymbol{\alpha}}_f &= \begin{bmatrix}0 & -5146.2 & -28342.0 & -5955.1 & 3822.2 & -18465.9\end{bmatrix}^T\text{ m} \\
t_f &= 2.5\text{ orbits}
\end{aligned}. \tag{24}$$

After precompensation and rotation into the $\Delta\delta\tilde{\boldsymbol{e}}$ plane using a counterclockwise rotation through $\omega = 15^o$ about the origin, the desired in-plane change is given by

$$a\Delta\delta\bar{\boldsymbol{a}}_{des} = \begin{bmatrix}0 & -4387.9 & -21063.3 & 209.9\end{bmatrix}^T\text{ m}. \tag{25}$$

Using Tables 2 and 3 to find the reachable delta-v minimum for the reconfiguration in Eq. (24) yields $\delta v_{min,MMS} = 1.3390$ m/s which is equal to $\delta v_{min,\delta\boldsymbol{e}}$. Therefore, the example reconfiguration is dominant $\delta\boldsymbol{e}$. Applying Koenig's algorithm gives a global minimum delta-v $\delta v_{lb} = 1.3392$ m/s. The reachable delta-v minimum matches up to 0.2 mm/s (0.014%), which is likely the result of Koenig's algorithm's use of a tolerance to stop iterations. From there, using column 3 in Table 8 T_{opt} is found to be [4.27812, 8.59431, 12.8735, 17.1897, 21.4690] $\times 10^4 s$. The points in the corresponding nested reachable set $S_n^*(\delta v_{min,\delta\boldsymbol{e}}, T_{opt})$, calculated using Eq. (6), are given by

$$S_n = \begin{bmatrix}
11586 & -115846 & 11586 & -115846 & 11586 \\
-218884 & 1637866 & -109690 & 546040 & -498 \\
-20399 & -20399 & -20399 & -20399 & -20399 \\
-5248 & -5248 & -5248 & -5248 & -5248
\end{bmatrix}\text{ m}, \tag{26}$$

where each column represents a 4D vector of the in-plane change in ROE ($a\Delta\delta\bar{\boldsymbol{\alpha}}_{des}$) achieved using the optimal maneuver $\delta\boldsymbol{v}^*$, given in Eq. (12). There are two possible sets of three maneuvers that satisfy the Type 1 constraints in column 3 of Table 9 for the desired change in ROE. From that set, suppose the maneuvers are chosen to occur at $t_1 = 42781.2$ s, $t_2 = 171897$ s, and $t_3 = 214690$ s, which correspond to the first, fourth, and fifth columns of Eq. (26). Using the 4th column of Table 9, the maneuvers are calculated to be

$$\begin{aligned}
\delta\boldsymbol{v}_1 &= \begin{bmatrix}0.00123 & 0.3285 & 0\end{bmatrix}^T\text{ m/s at } t_1 = 42781.2\text{ s} \\
\delta\boldsymbol{v}_2 &= \begin{bmatrix}0.00026 & -0.12173 & 0\end{bmatrix}^T\text{ m/s at } t_2 = 171897\text{ s} \\
\delta\boldsymbol{v}_3 &= \begin{bmatrix}0.00332 & 0.888743 & 0\end{bmatrix}^T\text{ m/s at } t_3 = 214690\text{ s}
\end{aligned} \tag{27}$$

which has a 2-norm total delta-v equal to the delta-v minimum. Figure 12 shows the resulting evolution of the in-plane ROE with Keplerian effects only when the maneuvers in Eq. (27) are applied. Notice in Figure 12b, the dominant plane, the maneuvers point along the shortest path from the origin to the desired change in the relative eccentricity vector.

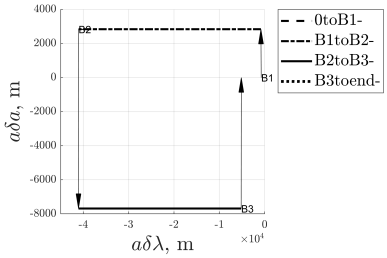

(a) Relative semi-major axis and relative mean longitude as affected by maneuvers (arrows) and Keplerian effects.

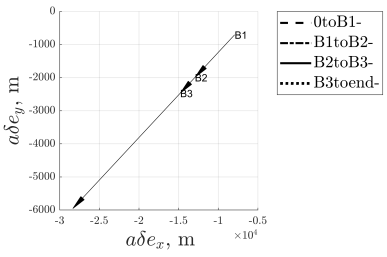

(b) Relative eccentricity vector as affected by maneuvers (arrows) and Keplerian effects.

Figure 12: Evolution of the ROE in Test 1, J_2 excluded from simulation

In addition, the reconfiguration error, defined as the 1-norm of the difference between the desired mean ROE and the achieved mean ROE, scaled by the desired mean ROE, is given in Table 12. The first row is the reconfiguration error for the case where the orbital elements are propagated numerically excluding J_2.

Table 12: Reconfiguration accuracy comparison, Test 1

Reconfiguration Error: achieved vs. desired ROE	**Relative orbit elements, (m)**			
	$a\delta a$	$a\delta\lambda$	$a\delta e_x$	$a\delta e_y$
J_2 excluded	0%	0.2261%	0.0001%	0.0000%
J_2 included, no precomp.	0%	8.0027%	0.0026%	0.0472%

The error is less than 1% in all ROE, so it is clear that the maneuver scheme in Eq. (27) achieves the desired ROE. It is worthwhile to determine how well the solutions perform in the presence of J_2. The second row of Table 12 reports the reconfiguration error between the desired and achieved mean ROE when the maneuver scheme in Eq. (27) is propagated using the numerical integration simulation including J_2. Because the maneuver scheme was calculated excluding J_2, propagating including J_2 yields errors, as expected, with the largest error in $\delta\lambda$. This motivates future work to further reduce the error by deriving closed-form solutions in eccentric orbits including J_2 effects. Nonetheless, for the first time in literature, this example demonstrated the ability of the new closed-form maneuver schemes to reconfigure an eccentric orbit with globally optimal delta-v.

Test 2: mDOT Mission out-of-plane reconfiguration in unperturbed, highly eccentric chief orbit. This example considers an out-of-plane reconfiguration in a highly eccentric geosynchronous transfer orbit in a mission to image Beta Pictoris with a miniaturized distributed occulter/telescope (mDOT). The mDOT mission is a formation flying mission which aims to directly image extrasolar dust and exoplanets to better understand how planets are formed.[26] The initial chief orbit is

$$\boldsymbol{\alpha}_{c,0} = \begin{bmatrix} 24500\text{ km} & 0.72 & 39^o & 357^o & 88^o & 0^o \end{bmatrix}^T. \tag{28}$$

To demonstrate the capability of the closed-form out-of-plane maneuver schemes (in Table 8 and 9) to reconfigure a relative orbit with minimum delta-v, the out-of-plane reconfiguration parameters are given by[15]

$$\begin{aligned} \delta\bar{\boldsymbol{\alpha}}_0 &= \begin{bmatrix} -4910 & -442840 \end{bmatrix}^T \text{ m} \\ \delta\bar{\boldsymbol{\alpha}}_f &= \begin{bmatrix} -4620 & -442850 \end{bmatrix}^T \text{ m} \cdot \\ t_f &= 1 \text{ orbit} \end{aligned} \tag{29}$$

The desired out-of-plane change after precompensation and counterclockwise rotation through $\omega = 88^o$ is

$$a\Delta\delta\bar{\boldsymbol{a}}_{des} = \begin{bmatrix} 0.1269 & -290.1723 \end{bmatrix}^T \text{ m}. \tag{30}$$

Using Table 4, $\nu^* = -1.5704$ rad, which satisfies the condition in the third row of the table ($\nu' = \nu^*$ & $\nu' = \nu^* + \pi \notin (\nu_{re}, \nu_{dis})$). The reachable delta-v minimum for this reconfiguration is found using Table 4 to be $\delta v_{min,mDOT} = 0.0478$ m/s. From Table 9, this reconfiguration requires two maneuvers, which are calculated using Table 1 to be

$$\begin{aligned} \delta\boldsymbol{v}_1 &= \begin{bmatrix} 0 & 0 & -0.0239 \end{bmatrix}^T \text{ m/s at } t = 5167.8 \text{ s} \\ \delta\boldsymbol{v}_2 &= \begin{bmatrix} 0 & 0 & 0.0239 \end{bmatrix}^T \text{ m/s at } t = 32996.7 \text{ s}. \end{aligned} \tag{31}$$

The total maneuver scheme cost closely matches the output of Koenig's algorithm, $\delta v_{lb} = 0.0477$ m/s with an error of 0.2%, therefore the closed-form maneuver scheme is globally optimal. Again, the error is likely numerical or due to the chosen tolerance. Figure 13 shows the evolution of the out-of-plane ROE when the maneuvers in Eq. (31) are applied.

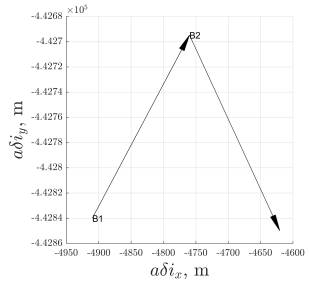

Figure 13: Relative inclination vector as affected by maneuvers (arrows) and Keplerian effects.

Notice that the maneuvers do not follow the shortest geometric path from initial to final relative inclination vector. This is because the desired pseudo-state lies in the disconnected region in the $\Delta\delta\boldsymbol{i}$ reachable set.

The first row of Table 13 is the reconfiguration error when the orbital elements are propagated using numerical integration including only Keplerian effects.

Table 13: Reconfiguration accuracy comparison, Test 2

Reconfiguration Error: achieved vs. desired ROE	**Relative orbit elements, (m)**	
	$a\delta i_x$	$a\delta i_y$
J_2 excluded	0.0060%	0.0000%
J_2 included, no precomp.	0.0067%	0.00013%

The error is about 0%, which confirms that in the presence of only Keplerian effects, the maneuver in Eq. (31) achieves the desired out-of-plane ROE change. As in Test 1, the second row of Table 13 gives the reconfiguration error between the desired and achieved mean ROE when the maneuver scheme in Eq. (31) is propagated using numerical integration including J_2 effects. The error, as expected, is nonzero, but significantly lower than the error in the in-plane ROE in Test 1. In fact, the error is very small when the inclination of the chief is small, because the effect of J_2 is scaled by $\sin^2(i)$ (see Eq. (32)). In addition, this is a very short reconfiguration, so there is not enough time to accumulate significant drift in the relative inclination vector.

SUMMARY

The applicability of the globally optimal closed-form maneuver schemes in this paper is driven by the nested reachable set of a given reconfiguration's dominance case. The dominance case is determined by choosing the maximum of all reachable delta-v minima in Tables 1-4 for eccentric chief orbits or in Tables 5-7 for near-circular orbits. Once the dominance case is known, the nested reachable set is computed with Eq. (7) using the corresponding $\delta\boldsymbol{v}^*$ and ν_{opt} or T_{opt} given in Table 8 for eccentric orbits and in Table 10 for near-circular orbits. Using the nested reachable sets (shown in Figures 8-9), the closed-form maneuver schemes for each dominance case can be sorted into three categories. First, if the nested reachable set contains all pseudo-states in the reachable set in the non-dominant plane, as in the near-circular dominant $\delta\boldsymbol{e}$ case, then the maneuver scheme applies to any reconfigurations for that dominance case. The same is true if the number of state variables is the same as the dimension of the nested reachable set, as in the near-circular and eccentric dominant $\delta\boldsymbol{i}$ cases, because there is no non-dominant plane. Second, if the nested reachable set only partially covers the reachable set in the non-dominant plane, as in the near-circular dominant δa and the eccentric dominant $\delta\boldsymbol{e}$ cases, then the maneuver scheme applies in a restricted range of reconfigurations for that dominance case. Finally, if the nested reachable set is extremely restricted, as in the eccentric dominant δa case and the near-circular and eccentric dominant $\delta\lambda$ cases, then the maneuver scheme is applicable in the dominant plane only. The closed-form maneuver schemes for the first two categories are given in Tables 8-9 for eccentric orbits, and in Tables 10-11 for near-circular orbits.

For the last category, the maneuver schemes are given in the Appendix in Tables 14-15.

CONCLUSION

To address the challenges of multi-spacecraft control, this paper presents new solutions to the satellite relative orbit reconfiguration problem of achieving a desired spacecraft end state in fixed-time. Though many authors have attempted to solve the satellite relative orbit reconfiguration problem using numerical methods, there are still unanswered questions in the space of closed-form solutions, despite their inherent efficiency. Typically, closed-form solutions are only employed to solve simple, specific problems. However, this paper leverages the geometric advantages of reachable set theory to derive closed-form, globally optimal impulsive maneuver schemes in cases that have yet been addressed in literature.

The relative orbit reconfiguration problem is cast in relative orbit element space, which inherently allows for the linearization of the dynamics equations that govern relative motion and the straight-forward inclusion of perturbations. The dynamics are discretized using a state transition matrix, which propagates the state forward in time, and a control input matrix derived from the Gauss Variational Equations, which represents the effect on the state of an impulsive maneuver with components in the radial, tangential, and normal directions.

Reachable set theory defines the reachable set S^* as a geometric relative orbit element space that can be achieved with multiple maneuvers in specified finite time with a specified total cost. The reachable set scales linearly with cost, and allows for the geometric visualization of optimality conditions. An optimal reconfiguration cost is defined as the cost for which the desired pseudo-state lies on the boundary of S^*. It is shown that optimality can be assessed according to this criteria and without loss of generality by projecting a general $2n$-dimensional reconfiguration into n 2D planes. This motivates the derivation of the δv_{min}, a new optimality metric whose reachability is quantifiable. The minimum delta-v required to achieve the entire desired reconfiguration cannot be less than the maximum of the set of minimum delta-vs required to achieve each 2D reconfiguration independently. The plane that drives δv_{min} is called the dominant plane, and the other 2D planes are called non-dominant. It is shown that δv_{min} is exactly equal to the delta-v required by the dominant plane reconfiguration if the desired pseudo-state lies in the nested reachable set, the set formed by mapping the optimal times and maneuvers for the dominant change onto the non-dominant planes. A general methodology to derive the δv_{min} is presented and then applied specifically to the ROE state representation for each dominance case.

Next, a general methodology is presented for use in computing maneuver schemes that meet the aforementioned optimality criteria while achieving a prescribed reconfiguration. The optimal maneuvers and maneuver locations are derived and used to define the nested reachable sets in the non-dominant planes or equivalently, the range of reconfigurations for which δv_{min} is reachable. The reachability of the δv_{min} for each dominance case is quantified by then analyzing the nested reachable sets in the non-dominant planes. According to the results of this analysis, the explicit expressions for all possible maneuver schemes that are achievable with minimum delta-v in each dominance case are presented. For the first time in literature, this paper presents general, closed-form, globally-optimal maneuver schemes for eccentric chief orbits. For two examples in eccentric orbits based on real missions, the maneuver schemes are validated to show that they achieve a desired reconfiguration and do so optimally.

The new maneuver schemes apply in the case where the desired reconfiguration lies within the nested reachable set in the dominant and non-dominant plane. However, there are reconfigurations where this is not true. For example, the optimal maneuvers may be linearly dependent, or a desired reconfiguration may not lie within the nested reachable set if the reconfiguration time is less than one orbit. This motivates future work to derive the closed form δv_{min} in cases not covered here, and to use this metric to derive maneuver schemes applicable to shorter or more restrictive reconfigurations. In addition, the algorithms here are limited to J_2 perturbed near-circular orbits and unperturbed eccentric orbits. Inclusion of other perturbations such as solar radiation pressure, solar/lunar third body, and atmospheric drag has not yet been addressed, but the algorithms presented in this paper can be used as an initial guess in a numerical approach to significantly reduce the number of iterations.

APPENDIX A: DYNAMICS OF RELATIVE MOTION

The state transition matrix for the quasi-nonsingular ROE is given by

$$\boldsymbol{\Phi}(t_f,t_0)=\begin{bmatrix} 1 & 0 & 0 & 0 & 0 & 0\\ -\frac{7}{2}\kappa\eta P\tau-\frac{3}{2}n\tau & 1 & 7\kappa e_{x0}P\tau & 7\kappa e_{y0}P\tau & -7\kappa\eta S\tau & 0\\ \frac{7}{2}\kappa e_{yf}Q\tau & 0 & \cos(\dot\omega\tau)-4\kappa e_{x0}e_{yf}GQ\tau & -\sin(\dot\omega\tau)-4\kappa e_{y0}e_{yf}GQ\tau & 5\kappa e_{yf}S\tau & 0\\ -\frac{7}{2}\kappa e_{xf}Q\tau & 0 & \sin(\dot\omega\tau)+4\kappa e_{x0}e_{xf}GQ\tau & \cos(\dot\omega\tau)+4\kappa e_{y0}e_{xf}GQ\tau & -5\kappa e_{xf}S\tau & 0\\ 0 & 0 & 0 & 0 & 1 & 0\\ \frac{7}{2}\kappa S\tau & 0 & -4\kappa e_{x0}GS\tau & -4\kappa e_{y0}GS\tau & 2\kappa T\tau & 1 \end{bmatrix}, \tag{32}$$

where

$$\begin{array}{llll} \gamma=\frac{3}{4}J_2R_e^2\sqrt{\mu}, & \eta=\sqrt{1-||\boldsymbol{e}||^2}, & \kappa=\frac{\gamma}{a^{\frac{7}{2}}\eta^4} & G=\frac{1}{\eta^2}\\ E=1+\eta, & F=4+3\eta, & T=\sin^2 i & \tau=t_f-t_0.\\ P=3\cos^2 i-1, & Q=5\cos^2 i-1, & S=\sin 2i & \dot\omega=\kappa Q \end{array} \tag{33}$$

The subscripts 0 and f denote initial and final values of the chief's orbit elements, respectively, and e_x, e_y are the x, y components of the absolute eccentricity vector. μ is the Earth's gravitational parameter, R_e is the Earth's equatorial radius, and n is the mean motion of the chief spacecraft. The STM in Eq. (32) includes only the dominant effects of J_2 on the relative dynamics.

Perturbed Near-circular Orbits

If the chief orbit has zero eccentricity ($e_c=0$), the STM in Eq. (32) reduces to

$$\boldsymbol{\Phi}(t_f,t_0)=\begin{bmatrix} 1 & 0 & 0 & 0 & 0 & 0\\ -\frac{7\kappa EP+3n}{2}\tau & 1 & 0 & 0 & -\kappa FS\tau & 0\\ 0 & 0 & \cos(\dot\omega\tau) & -\sin(\dot\omega\tau) & 0 & 0\\ 0 & 0 & \sin(\dot\omega\tau) & \cos(\dot\omega\tau) & 0 & 0\\ 0 & 0 & 0 & 0 & 1 & 0\\ \frac{7}{2}\kappa S\tau & 0 & 0 & 0 & 2\kappa T\tau & 1 \end{bmatrix}. \tag{34}$$

It is convenient to use the mean argument of latitude $u=M+\omega$ in place of time as the independent variable. The equivalent STM is found by replacing τ, the time interval with

$$\tau=\frac{\Delta u}{n+\kappa(\eta P+Q)}, \tag{35}$$

which describes the relationship between time and the mean argument of latitude in the presence of secular J_2 effects. Adapting Eq. (4) to near-circular orbits, the effect of an impulsive maneuver $\delta\boldsymbol{v}_k$ at u_k on the ROE is given by

$$\Delta\delta\boldsymbol{\alpha}_k=\boldsymbol{\Gamma}_k\delta\boldsymbol{v}_k=\frac{1}{na}\begin{bmatrix} 0 & 2 & 0\\ -2 & 0 & 0\\ \sin(u_k) & 2\cos(u_k) & 0\\ -\cos(u_k) & 2\sin(u_k) & 0\\ 0 & 0 & \cos(u_k)\\ 0 & 0 & \sin(u_k) \end{bmatrix}\begin{bmatrix}\delta v_R\\ \delta v_T\\ \delta v_N\end{bmatrix}. \tag{36}$$

Unperturbed Eccentric Orbits

For unperturbed eccentric orbits, the STM in Eq. (32) reduces to

$$\boldsymbol{\Phi}(t_f,t_0)=\begin{bmatrix} 1 & 0 & 0 & 0 & 0 & 0\\ -\frac{3}{2}\Delta M & 1 & 0 & 0 & 0 & 0\\ 0 & 0 & 1 & 0 & 0 & 0\\ 0 & 0 & 0 & 1 & 0 & 0\\ 0 & 0 & 0 & 0 & 1 & 0\\ 0 & 0 & 0 & 0 & 0 & 1 \end{bmatrix} \tag{37}$$

in the presence of only Keplerian effects, where the time interval has been replaced with the change in mean anomaly $\Delta M = M_f - M_0$. The effects of an impulsive maneuver $\delta\boldsymbol{v}_k$ at true argument of latitude $\theta_k = \nu_k + \omega_k$ are given by[7]

$$\Delta\delta\boldsymbol{\alpha}_k = \boldsymbol{\Gamma}_k\delta\boldsymbol{v}_k = \frac{1}{na}\begin{bmatrix} \frac{2}{\eta}e\sin\nu_k & \frac{2}{\eta}(1+e\cos\nu_k) & 0 \\ -\frac{2\eta^2}{1+e\cos\nu_k} & 0 & 0 \\ \eta\sin\theta_k & \eta\frac{(2+e\cos\nu_k)\cos\theta_k+e_x}{1+e\cos\nu_k} & \frac{\eta e_y}{\tan(i)}\frac{\sin\theta_k}{1+e\cos\nu_k} \\ -\eta\cos\theta_k & \eta\frac{(2+e\cos\nu_k)\sin\theta_k+e_y}{1+e\cos\nu_k} & -\frac{\eta e_x}{\tan(i)}\frac{\sin\theta_k}{1+e\cos\nu_k} \\ 0 & 0 & \eta\frac{\cos\theta_k}{1+e\cos\nu_k} \\ 0 & 0 & \eta\frac{\sin\theta_k}{1+e\cos\nu_k} \end{bmatrix}\begin{bmatrix}\delta v_R \\ \delta v_T \\ \delta v_N\end{bmatrix}. \tag{38}$$

APPENDIX B: OTHER CLOSED-FORM SOLUTIONS

The tables below present closed-form globally optimal maneuvers schemes in near-circular and eccentric for cases where only the desired change in the dominant plane is important.

The General Methodology is the same as for the other closed-form solutions presented in this paper. The optimal times and maneuvers are computed for a given dominance case using Table 14.

Table 14: Optimal maneuver vectors $\delta\boldsymbol{v}^*$ and optimal maneuver times T_{opt} for dominant-plane-only reconfigurations

Region	$\delta\boldsymbol{v}^*$, (m/s)	T_{opt}, (s)
Dominant δa, ecc.	$\Delta\delta a > 0:\ \delta\boldsymbol{v}^* = \begin{bmatrix}0 & +\delta v_{min,\delta a} & 0\end{bmatrix}^T$ for all i $\Delta\delta a < 0:\ \delta\boldsymbol{v}^* = \begin{bmatrix}0 & -\delta v_{min,\delta a} & 0\end{bmatrix}^T$	$k2\pi$, $k = \text{floor}(\frac{\nu_f}{2\pi})$
Dominant $\delta\lambda$, ecc.	$\begin{bmatrix}0 & \pm 1 & 0\end{bmatrix}^T$ $\begin{bmatrix}\frac{e\sin(\nu_t)}{\sqrt{e^2+2e\cos(\nu_t)+1}} & \mp\frac{1+e\cos(\nu_t)}{\sqrt{e^2+2e\cos(\nu_t)+1}} & 0\end{bmatrix}^T$ for $\mp\Delta\delta\bar{\lambda}_{des}$	0 ν_t
Dominant $\delta\lambda$, near-circ.	$\begin{bmatrix}0 & \pm 1 & 0\end{bmatrix}^T$ $\begin{bmatrix}0 & \mp 1 & 0\end{bmatrix}^T$ for $\mp\Delta\delta\bar{\lambda}_{des}$	0 u_f

Then, a subset of S_n, the nested reachable set, is chosen such that the maneuvers satisfy the constraints given in the third column of Table 15. There are fewer constraints for these cases because the effects of the maneuvers in the non-dominant planes is not considered.

Table 15: Closed-form maneuver scheme constraints in dominant-plane-only reconfigurations

Region	**# of Maneuvers**	**Constraints (Type 1)**	**Linear System**
Dominant δa, ecc.			
	1	$a\Delta\delta\bar{\lambda}_{des} = \frac{\mp 3}{\eta n}(M_f - k2\pi)(1+e)$ for $\pm\Delta\delta\bar{a}_{des}$	$c_1 = 1$
	2	$a\Delta\delta\bar{\lambda}_{des} \neq \frac{\mp 3}{\eta n}(M_f - k2\pi)(1+e)$ for $\pm\Delta\delta\bar{a}_{des}$	$\sum_{i=1}^{2} c_i = 1$ $\sum_{i=1}^{2} c_i a\Delta\delta\lambda_i = a\Delta\delta\bar{\lambda}_{des}$
Dominant $\delta\lambda$, ecc.	2	N/A	$\sum_{i=1}^{2} c_i a\Delta\delta a_i = a\Delta\delta\bar{a}_{des}$ $\sum_{i=1}^{2} c_i a\Delta\delta\lambda_i = a\Delta\delta\bar{\lambda}_{des}$
Dominant $\delta\lambda$, near-circ.	2	N/A	$\sum_{i=1}^{2} c_i a\Delta\delta a_i = a\Delta\delta\bar{a}_{des}$ $\sum_{i=1}^{2} c_i a\Delta\delta\lambda_i = a\Delta\delta\bar{\lambda}_{des}$

APPENDIX C: NOTES ON DOMINANT RELATIVE SEMI-MAJOR AXIS SOLUTIONS IN NEAR-CIRCULAR ORBITS

To ensure that a convex combination exists, the desired pseudo-state in $\delta\lambda$ must satisfy

$$\begin{array}{l} \frac{(\Delta\delta\lambda_3-\Delta\delta\lambda_2)(\pm||\Delta\delta\boldsymbol{e}_{des}||)+(\Delta\delta\bar{\lambda}_{des}-\Delta\delta\lambda_3)(\pm||\Delta\delta\boldsymbol{e}_2||)+(\Delta\delta\lambda_2-\Delta\delta\bar{\lambda}_{des})(\pm||\Delta\delta\boldsymbol{e}_3||)}{d(\Delta\delta\bar{\boldsymbol{\alpha}}_{des})} \geq 0 \\ \frac{(\Delta\delta\lambda_3-\Delta\delta\bar{\lambda}_{des})(\pm||\Delta\delta\boldsymbol{e}_1||)+(\Delta\delta\lambda_1-\Delta\delta\lambda_3)(\pm||\Delta\delta\bar{\boldsymbol{e}}_{des}||)+(\Delta\delta\bar{\lambda}_{des}-\Delta\delta\lambda_1)(\pm||\Delta\delta\boldsymbol{e}_3||)}{d(\Delta\delta\bar{\boldsymbol{\alpha}}_{des})} \geq 0 \\ \frac{(\Delta\delta\bar{\lambda}_{des}-\Delta\delta\lambda_2)(\pm||\Delta\delta\boldsymbol{e}_1||)+(\Delta\delta\lambda_1-\Delta\delta\bar{\lambda}_{des})(\pm||\Delta\delta\boldsymbol{e}_2||)+(\Delta\delta\lambda_2-\Delta\delta\lambda_1)(\pm||\Delta\delta\bar{\boldsymbol{e}}_{des}||)}{d(\Delta\delta\bar{\boldsymbol{\alpha}}_{des})} \geq 0 \end{array} \tag{39}$$

$d(\Delta\delta\bar{\boldsymbol{\alpha}}_{des}) = (\Delta\delta\lambda_3 - \Delta\delta\lambda_2)(\pm||\Delta\delta\boldsymbol{e}_1||) + (\Delta\delta\lambda_1 - \Delta\delta\lambda_3)(\pm||\Delta\delta\boldsymbol{e}_2||) + (\Delta\delta\lambda_2 - \Delta\delta\lambda_1)(\pm||\Delta\delta\boldsymbol{e}_3||).$

REFERENCES

[1] S. D'Amico, M. Pavone, S. Saraf, A. Alhussien, T. Al-Saud, S. Buchman, R. Byer, and C. Farhat, "Miniaturized Autonomous Distributed Space System for Future Science and Exploration," 8th International Workshop on Satellite Constellations and Formation Flying, IWSCFF 2015, Delft University of Technology, June 8-10, 2015.

[2] A. Ichikawa and Y. Ichimura, "Optimal Impulsive Relative Orbit Transfer Along a Circular Orbit," *Journal of Guidance, Control, and Dynamics*, Vol. 31, No. 4, 2008, pp. 1014–1027, https://doi.org/10.2514/1.32820.

[3] M. Khalil, B. Larbi, and E. Stoll, "Spacecraft Formation Control using Analytical Integration of Gauss' Variational Equations," 6th International Conference on Astrodynamics Tools and Techniques - ICATT, Darmstadt, Germany, March 2016.

[4] S. D'Amico, "Relative Orbital Elements as Integration Constants of Hill's Equations," 2005. DLR-GSOC TN 05-08; Deutsches Zentrum für Luft- und Raumfahrt, Oberpfaffenhofen.

[5] G. Gaias and S. D'Amico, "Impulsive Maneuvers for Formation Reconfiguration Using Relative Orbital Elements," *Journal of Guidance, Control and Dynamics*, Vol. 38, No. 6, 2015, pp. 1036–1049, 10.2514/1.G000189.

[6] G. Gaias, S. D'Amico, and J.-S. Ardaens, "Generalized Multi-Impulsive Maneuvers for Optimum Spacecraft Rendezvous in Near-Circular Orbit," *International Journal of Space Science and Engineering*, Vol. 3, No. 1, 2015, pp. 68–88, 10.1504/IJSPACESE.2015.069361.

[7] M. Chernick and S. D'Amico, "New Closed-Form Solutions for Optimal Impulsive Control of Spacecraft Relative Motion," *Journal of Guidance, Control and Dynamics*, Vol. 41, No. 2, 2018, pp. 301–319.

[8] S. Vaddi, K. Alfriend, S. Vadali, and P. Sengupta, "Formation Establishment and Reconfiguration Using Impulsive Control," *Journal of Guidance, Control and Dynamics*, Vol. 28, 03 2005, pp. 262–268.

[9] H. Schaub and K. Alfriend, "Impulsive Feedback Control to Establish Specific Mean Orbit Elements of Spacecraft Formations," *Journal of Guidance Control and Dynamics*, Vol. 24, 07 2001, pp. 739–745.

[10] J. Betts, "Survey of Numerical Methods for Trajectory Optimization," *Journal of Guidance, Control and Dynamics*, Vol. 21, No. 2, 1998, pp. 193–207.

[11] L. Sobiesiak and C. Damaren, "Impulsive Spacecraft Formation Maneuvers with Optimal Firing Times," *Journal of Guidance, Control and Dynamics*, Vol. 38, No. 10, 2015, pp. 1994–2000.

[12] C. Roscoe, J. Westphal, J. Griesbach, and H. Schaub, "Formation Establishment and Reconfiguration Using Differential Elements in J_2-Perturbed Orbits," *Journal of Guidance, Control and Dynamics*, Vol. 38, 2015, p. 1725–1740.

[13] J. Prussing, *Primer Vector Theory and Applications, In: Conway, B.A. (ed.) Spacecraft Trajectory Optimization*. Cambridge University Press, Cambridge, 2011. pp. 15–35.

[14] E. Gilbert and G. Harasty, "A class of fixed-time fuel-optimal impulsive control problems and an efficient algorithm for their solution," *IEEE Transactions on Automatic Control*, Vol. 16, Feb 1971, pp. 1–11, 10.1109/TAC.1971.1099656.

[15] A. Koenig and S. D'Amico, "Real-Time Algorithm for Globally Optimal Impulsive Control of Linear Time-Variant Systems," *IEEE Transactions on Automatic Control*, 2018. Submitted, http://arxiv.org/abs/1804.06099.

[16] R. E. Allen, A. A. Clark, J. A. Starek, and M. Pavone, "A machine learning approach for real-time reachability analysis," *2014 IEEE/RSJ International Conference on Intelligent Robots and Systems*, Sept 2014, pp. 2202–2208, 10.1109/IROS.2014.6942859.

[17] S. D'Amico and O. Montenbruck, "Proximity Operations of Formation Flying Spacecraft using an Eccentricity/Inclination Vector Separation," *Journal of Guidance, Control and Dynamics*, Vol. 29, No. 3, 2006, pp. 554–563.

[18] S. D'Amico, S. D. Florio, R. Larsson, and M. Nylund, "Autonomous Formation Keeping and Reconfiguration for Remote Sensing Spacecraft," 21st International Symposium on Space Flight Dynamics. 28 Sep. -2 Oct. 2009, Toulouse, France (2009).

[19] J.-S. Ardaens and D. Fischer, "TanDEM-X Autonomous Formation Flying System: Flight Results," *IFAC Proceedings Volumes*, Vol. 44, No. 1, 2011, pp. 709 – 714. 18th IFAC World Congress.

[20] A. Koenig, T. Guffanti, and S. D'Amico, "New State Transition Matrices for Spacecraft Relative Motion in Perturbed Orbits," *Journal of Guidance, Control, and Dynamics*, Vol. 40, 9 2017, pp. 1749–1768.

[21] D. Brouwer, "Solution of the problem of artificial satellite theory without drag," Vol. 64, 10 1959, p. 378.

[22] F. d. Bruijn, E. Gill, and J. How, "Comparative Analysis of Cartesian and Curvilinear Clohessy-Wiltshire Equations," *Journal of Aerospace Engineering, Sciences and Applications*, Vol. 3, 05 2011, pp. 1–15.

[23] K. Yamanaka and F. Ankerson, "New State Transition Matrix for Relative Motion on an Arbitrary Elliptical Orbit," *Journal of Guidance, Control and Dynamics*, Vol. 25, 2002, pp. 60–66.

[24] R. Garner, "MMS - Magnetospheric Multiscale," Feb 2015.

[25] A. Koenig, S. D'Amico, B. Macintosh, and C. Titus, "Optimal Formation Design of a Miniaturized Distributed Occulter/Telescope in Earth Orbit," 2015 AAS/AIAA Astrodynamics Specialist Conference, Vail, Colorado, August 9-13, 2015.

[26] J. Kolmas, P. Banazadeh, A. Koenig, S. D'Amico, and B. Macintosh, "System Design of a Miniaturized Distributed Occulter/Telescope for Direct Imaging of Star Vicinity," IEEE Aerospace Conference, Yellowstone Conference Center, Big Sky, Montana, March 5-12, 2016.

[27] S. Hughes, "Formation Design and Sensitivity Analysis for the Magnetospheric Multiscale Mission (MMS)," *AIAA/AAS Astrodynamics Specialist Conference and Exhibit*, 2008, 10.2514/6.2008-7357.

[28] C. W. Roscoe, S. R. Vadali, K. T. Alfriend, and U. P. Desai, "Satellite formation design in orbits of high eccentricity with performance constraints specified over a region of interest: MMS phase II," *Acta Astronautica*, Vol. 82, No. 1, 2013, pp. 16 – 24. 6th International Workshop on Satellite Constellation and Formation Flying, https://doi.org/10.1016/j.actaastro.2012.07.028.

[29] M. Volle, T. Lee, A. Long, C. Gramling, and J. Carpenter, "Maneuver Recovery Analysis for the Magnetospheric Multiscale Mission," *NASA Technical Reports Server*, 2007.